

1 Erosion of somatic tissue identity with loss of the X-linked  
2 intellectual disability factor KDM5C

3

4 Katherine M. Bonefas<sup>1,2</sup>, Ilakkia Venkatachalam<sup>2,3</sup>, and Shigeki Iwase<sup>2</sup>.

5 1. Neuroscience Graduate Program, University of Michigan Medical School, Ann Arbor, MI, 48109, USA.

6      2. Department of Human Genetics, Michigan Medicine, University of Michigan Medical School, Ann Arbor,  
7           MI, 48109, USA.

8 3. Genetics and Genomics Graduate Program, University of Michigan, Ann Arbor, MI, 48109, USA.

## 9 Abstract

10 Mutations in numerous chromatin-modifying enzymes cause neurodevelopmental disorders (NDDs)  
11 with unknown mechanisms. Loss of repressive chromatin regulators can lead to the aberrant transcription  
12 of tissue-specific genes outside of their intended context, however the mechanisms and consequences  
13 of their dysregulation are largely unknown. Here, we examine how lysine demethylase 5c (KDM5C), an  
14 eraser of histone 3 lysine 4 di and tri-methylation (H3K4me2/3) mutated in Claes-Jensen X-linked intellectual  
15 disability, contributes to tissue identity. We found male *Kdm5c* knockout (-KO) mice, which recapitulate  
16 key human neurological phenotypes, aberrantly expresses many liver, muscle, ovary, and testis genes  
17 within the amygdala and hippocampus. Gonad-enriched genes misexpressed in the *Kdm5c*-KO brain are  
18 unique to germ cells, indicating an erosion of the soma-germline boundary. Germline genes are typically  
19 decommissioned in somatic lineages in the post-implantation epiblast, yet *Kdm5c*-KO epiblast-like cells  
20 (EpiLCs) aberrantly expressed key regulators of germline identity and meiosis, including *Dazl* and *Stra8*.  
21 Germline gene suppression is sexually dimorphic, as female EpiLCs required a higher dose of KDM5C  
22 to maintain germline gene suppression. Using a comprehensive list of mouse germline-enriched genes,  
23 we found KDM5C is selectively recruited to a subset of germline gene promoters that contain CpG islands  
24 (CGIs) to facilitate DNA CpG methylation (CpGme) during ESC to EpiLC differentiation. However, late stage  
25 spermatogenesis genes devoid of promoter CGIs can also become activated in *Kdm5c*-KO cells via ectopic  
26 activation by RFX transcription factors. Together, these data indicate that KDM5C decommissions germline  
27 genes by facilitating CGI methylation to prevent runaway activation of germline developmental programs in  
28 somatic lineages.

## 29 Introduction

30 A single genome holds the instructions to generate the myriad of cell types found within an organism.  
31 This is, in part, accomplished by chromatin regulators that can either promote or impede lineage-specific  
32 gene expression through DNA and histone modifications<sup>1–5</sup>. Human genetic studies revealed mutations in  
33 chromatin regulators are a major cause of neurodevelopmental disorders (NDDs)<sup>6</sup> and many studies have  
34 identified their importance for regulating brain-specific transcriptional programs. Loss of chromatin regulators  
35 can also result in the ectopic expression of tissue-specific genes outside of their target environment, such  
36 as the misexpression of liver-specific genes within adult neurons<sup>7</sup>. However, the mechanisms underlying  
37 ectopic gene expression and its impact upon neurodevelopment are poorly understood.

38 To elucidate the role of tissue identity in chromatin-linked NDDs, it is essential to first characterize the  
39 nature of the dysregulated genes and the molecular mechanisms governing their de-repression. Here we  
40 focus on lysine demethylase 5C (KDM5C, also known as SMCX or JARID1C), which erases histone 3 lysine  
41 4 di- and trimethylation (H3K4me2/3), a permissive chromatin modification enriched at gene promoters<sup>8</sup>.  
42 Pathogenic mutations in *KDM5C* cause Intellectual Developmental Disorder, X-linked, Syndromic, Claes-  
43 Jensen Type (MRXSCJ, OMIM: 300534). MRXSCJ is more common and severe in males and its neurological  
44 phenotypes include intellectual disability, seizures, aberrant aggression, and autistic behaviors<sup>9–11</sup>. Male  
45 *Kdm5c* knockout (-KO) mice recapitulate key MRXSCJ phenotypes, including hyperaggression, increased  
46 seizure propensity, and learning impairments<sup>12,13</sup>. RNA sequencing (RNA-seq) of the *Kdm5c*-KO hippocam-  
47 pus revealed ectopic expression of some germline genes within the brain<sup>13</sup>. However, it is unclear if other  
48 tissue-specific genes are aberrantly transcribed with KDM5C loss, at what point in development germline  
49 gene misexpression begins, and what mechanisms underlie their dysregulation.

50 Distinguishing between germ cells and somatic cells is a key feature of multicellularity<sup>14</sup> that occurs  
51 during early embryogenesis in many metazoans<sup>15</sup>. In mammals, chromatin regulators are crucial for  
52 decommissioning germline genes during the transition from naïve to primed pluripotency. Initially, germline  
53 gene promoters gain repressive histone H2A lysine 119 monoubiquitination (H2AK119ub1)<sup>16</sup> and histone 3  
54 lysine 9 trimethylation (H3K9me3)<sup>16,17</sup> in embryonic stem cells (ESCs) and are then decorated with DNA  
55 CpG methylation (CpGme) in the post-implantation embryo<sup>17–20</sup>. The contribution of KDM5C to this process  
56 remains unclear. Furthermore, studies on germline gene repression have primarily been conducted in  
57 males and focused on marker genes important for germ cell development rather than germline genes as a  
58 whole, given the lack of a curated germline-enriched gene list. Therefore, it is unknown if the mechanism  
59 of repression differs between sexes or for certain classes of germline genes, e.g. meiotic genes versus  
60 spermatid differentiation genes.

61 To illuminate KDM5C's role in tissue identity, here we characterized the aberrant expression of tissue-  
62 enriched genes within the *Kdm5c*-KO brain and epiblast-like stem cells (EpiLCs), an *in vitro* model of the  
63 post-implantation embryo. We curated a list of mouse germline-enriched genes, which enabled genome-wide

64 analysis of germline gene silencing mechanisms for the first time. Based on the data presented below, we  
65 propose KDM5C plays a fundamental, sexually dimorphic role in the development of tissue identity during  
66 early embryogenesis, including the establishment of the soma-germline boundary.

## 67 Results

### 68 **Tissue-enriched genes are aberrantly expressed in the *Kdm5c*-KO brain**

69 Previous RNA sequencing (RNA-seq) of the adult male *Kdm5c*-KO hippocampus revealed ectopic  
70 expression of some germline genes unique to the testis<sup>13</sup>. It is currently unknown if the testis is the only  
71 tissue type misexpressed in the *Kdm5c*-KO brain. We thus systematically tested whether other tissue-specific  
72 genes are misexpressed in the male brain with constitutive knockout of *Kdm5c* (*Kdm5c*<sup>-y</sup>, 5CKO)<sup>21</sup> by using  
73 a published list of mouse tissue-enriched genes<sup>22</sup>.

74 We found a large proportion of significantly upregulated genes (DESeq2<sup>23</sup>, log2 fold change > 0.5, q < 0.1)  
75 within the male *Kdm5c*-KO amygdala and hippocampus are non-brain, tissue-specific genes (Amygdala: 35%,  
76 Hippocampus: 24%) (Figure 1A-B). For both the amygdala and hippocampus, the majority of tissue-enriched  
77 differentially expressed genes (DEGs) were testis genes (Figure 1A-B). Even though the testis has the  
78 largest total number of tissue-biased genes (2,496 genes) compared to any other tissue, testis-biased DEGs  
79 were significantly enriched for both brain regions (Amygdala p = 1.83e-05, Odds Ratio = 5.13; Hippocampus  
80 p = 4.26e-11, Odds Ratio = 4.45, Fisher's Exact Test). An example of a testis-enriched gene misexpressed  
81 in the *Kdm5c*-KO brain is *FK506 binding protein 6* (*Fkbp6*), a known regulator of PIWI-interacting RNAs  
82 (piRNAs) and meiosis<sup>24,25</sup> (Figure 1C).

83 Interestingly, we also observed significant enrichment of ovary-biased DEGs in both the amygdala and  
84 hippocampus (Amygdala p = 0.00574, Odds Ratio = 18.7; Hippocampus p = 0.048, Odds Ratio = 5.88,  
85 Fisher's Exact) (Figure 1A-B). Ovary-enriched DEGs included *Zygotic arrest 1* (*Zar1*), which sequesters  
86 mRNAs in oocytes for meiotic maturation<sup>26</sup> (Figure 1D). Given that the *Kdm5c*-KO mice we analyzed are  
87 male, these data demonstrate that the ectopic expression of gonad-enriched genes is independent of  
88 organismal sex.

89 Although not consistent across brain regions, we also found significant enrichment of DEGs biased  
90 towards two non-gonadal tissues - the liver (Amygdala p = 0.04, Odds Ratio = 6.58, Fisher's Exact Test) and  
91 muscles (Hippocampus p = 0.01, Odds Ratio = 6.95, Fisher's Exact Test) (Figure 1A-B). *Apolipoprotein C-I*  
92 (*Apoc1*) a lipoprotein metabolism and transport gene, is among the liver-biased DEG derepressed in both  
93 the hippocampus and amygdala<sup>27</sup> and its brain overexpression has been implicated in Alzheimer's disease<sup>28</sup>  
94 (Figure 1E).

95 For all *Kdm5c*-KO tissue-enriched DEGs, aberrantly expressed mRNAs are polyadenylated and spliced  
96 into mature transcripts (Figure 1C-E). Of note, we observed little to no dysregulation of brain-enriched genes

97 (Amygdala p = 1, Odds Ratio = 1.22; Hippocampus p = 0.74, Odds Ratio = 1.22, Fisher's Exact), despite the  
98 fact these are brain samples and the brain has the second highest total number of tissue-enriched genes  
99 (708 genes). Altogether, these results suggest the aberrant expression of tissue-enriched genes within the  
100 brain is a major effect of KDM5C loss.

101 **Germline genes are misexpressed in the *Kdm5c*-KO brain**

102 *Kdm5c*-KO brain expresses testicular germline genes<sup>13</sup>, however the testis also contains somatic cells that  
103 support hormone production and germline functions. To determine if *Kdm5c*-KO results in ectopic expression  
104 of somatic testicular genes, we first evaluated the known functions of testicular DEGs through gene ontology.  
105 We found *Kdm5c*-KO testis-enriched DEGs had high enrichment of germline-relevant ontologies, including  
106 spermatid development (GO: 0007286, p.adjust = 6.2e-12) and sperm axoneme assembly (GO: 0007288,  
107 p.adjust = 2.45e-14) (Figure 2A).

108 We then evaluated testicular DEG expression in wild-type testes versus testes with germ cell depletion<sup>29</sup>,  
109 which was accomplished by heterozygous *W* and *Wv* mutations in the enzymatic domain of *c-Kit* (*Kit*<sup>W/Wv</sup>)<sup>30</sup>.  
110 Almost all *Kdm5c*-KO testis-enriched DEGs lost expression with germ cell depletion (Figure 2B). We then  
111 assessed testis-enriched DEG expression in a published single cell RNA-seq dataset that identified cell  
112 type-specific markers within the testis<sup>31</sup>. Some *Kdm5c*-KO testis-enriched DEGs were classified as specific  
113 markers for different germ cell developmental stages (e.g. spermatogonia, spermatocytes, round spermatids,  
114 and elongating spermatids), yet none marked somatic cells (Figure 2C). Together, these data demonstrate  
115 that the *Kdm5c*-KO brain aberrantly expresses germline genes but not somatic testicular genes, reflecting an  
116 erosion of the soma-germline boundary.

117 As of yet, research on germline gene silencing mechanisms has focused on a handful of key genes rather  
118 than assessing germline gene suppression genome-wide, due to the lack of a comprehensive gene list.  
119 We therefore generated a list of mouse germline-enriched genes using RNA-seq datasets of *Kit*<sup>W/Wv</sup> mice  
120 that included males and females at embryonic day 12, 14, and 16<sup>32</sup> and adult male testes<sup>29</sup>. We defined  
121 genes as germline-enriched if their expression met the following criteria: 1) their expression is greater than  
122 1 FPKM in wild-type gonads 2) their expression in any non-gonadal tissue of adult wild type mice<sup>22</sup> does  
123 not exceed 20% of their maximum expression in the wild-type germline, and 3) their expression in the germ  
124 cell-depleted gonads, for any sex or time point, does not exceed 20% of their maximum expression in the  
125 wild-type germline. These criteria yielded 1,288 germline-enriched genes (Figure 2D), which was hereafter  
126 used as a resource to globally characterize germline gene misexpression with *Kdm5c* loss (Supplementary  
127 table 1).

128 ***Kdm5c*-KO epiblast-like cells aberrantly express key regulators of germline identity**

129 Germ cells are typically distinguished from somatic cells soon after the embryo implants into the uterine  
130 wall<sup>33,34</sup>, when germline genes are silenced in epiblast stem cells that will form the somatic tissues<sup>35</sup>. This  
131 developmental time point can be modeled *in vitro* through differentiation of naïve embryonic stem cells  
132 (nESCs) into epiblast-like stem cells (EpiLCs) (Figure 3A)<sup>36,37</sup>. While some germline-enriched genes are  
133 also expressed in nESCs and in the 2-cell stage<sup>38–40</sup>, they are silenced as they differentiate into EpiLCs<sup>17,18</sup>.  
134 Therefore, we tested if KDM5C was necessary for the initial silencing of germline genes in somatic lineages  
135 by evaluating the impact of *Kdm5c* loss in male EpiLCs.

136 *Kdm5c*-KO cell morphology during ESC to EpiLC differentiation appeared normal (Figure 3B) and EpiLCs  
137 properly expressed markers of primed pluripotency, such as *Dnmt3b*, *Fgf5*, *Pou3f1*, and *Otx2* (Figure 3C). We  
138 then identified tissue-enriched DEGs in a RNA-seq dataset of wild-type and *Kdm5c*-KO EpiLCs<sup>41</sup> (DESeq2,  
139 log<sub>2</sub> fold change > 0.5, q < 0.1). Similar to the *Kdm5c*-KO brain, we observed general dysregulation of  
140 tissue-enriched genes, with the largest number of genes belonging to the brain and testis, although they  
141 were not significantly enriched (Figure 3D). Using our list of mouse germline-enriched genes assembled  
142 above, we found 68 germline genes were misexpressed in male *Kdm5c*-KO EpiLCs.

143 We then compared EpiLC germline DEGs to those expressed in the *Kdm5c*-KO brain to determine if  
144 germline genes are constitutively dysregulated or change over the course of development. The majority of  
145 germline DEGs were unique to either EpiLCs or the brain, with only *D1Pas1* and *Cyct* shared across all  
146 tissue/cell types (Figure 3E-F). EpiLC germline DEGs had particularly high enrichment of meiosis-related  
147 gene ontologies when compared to the brain (Figure 3G), such as meiotic cell cycle process (GO:1903046,  
148 p.adjust = 2.2e-07) and meiotic nuclear division (GO:0140013, p.adjust = 1.37e-07). While there was  
149 modest enrichment of meiotic gene ontologies in both brain regions, the *Kdm5c*-KO hippocampus primarily  
150 expressed late-stage spermatogenesis genes involved in sperm axoneme assembly (GO:0007288, p.adjust  
151 = 0.00621) and sperm motility (GO:0097722, p.adjust = 0.00612).

152 Notably, DEGs unique to *Kdm5c*-KO EpiLCs included key drivers of germline identity, such as *Stimulated*  
153 *by retinoic acid 8* (*Stra8*: log<sub>2</sub> fold change = 3.73, q = 2.17e-39) and *Deleted in azoospermia like* (*Dazl*:  
154 log<sub>2</sub> fold change = 3.36, q = 3.19e-12) (Figure 3H). These genes are typically expressed when primordial  
155 germ cells (PGCs) are committed to the germline fate and later in life to trigger meiotic gene expression  
156 programs<sup>42–44</sup>. Of note, some germline genes, including *Dazl*, are also expressed in the two-cell embryo<sup>39,45</sup>.  
157 However, we did not see derepression of two-cell stage-specific genes, like *Duxf3* (*Dux*) (log<sub>2</sub> fold change  
158 = -0.282, q = 0.337) and *Zscan4d* (log<sub>2</sub> fold change = 0.25, q = 0.381) (Figure 3H), indicating *Kdm5c*-KO  
159 EpiLCs do not revert back to a 2-cell state. Altogether, *Kdm5c*-KO EpiLCs express key drivers of germline  
160 identity and meiosis while the brain primarily expresses spermiogenesis genes, indicating germline gene  
161 misexpression mirrors germline development during the progression of somatic development.

162 **Female epiblast-like cells have increased sensitivity to germline gene misexpression**  
163 **with *Kdm5c* loss**

164 It is currently unknown if the misexpression of germline genes is influenced by sex, as previous studies  
165 on germline gene repressors have focused on male cells<sup>16,17,19,46,47</sup>. Sex is particularly pertinent in the case  
166 of KDM5C because it partially escapes X chromosome inactivation (XCI), resulting in a higher dosage in  
167 females<sup>48–51</sup>. We therefore explored the impact of chromosomal sex upon germline gene suppression by  
168 comparing their dysregulation in male *Kdm5c* hemizygous knockout (XY *Kdm5c*-KO, XY 5CKO), female  
169 homozygous knockout (XX *Kdm5c*-KO, XX 5CKO), and female heterozygous knockout (XX *Kdm5c*-HET, XX  
170 5CHET) EpiLCs<sup>41</sup>.

171 In EpiLCs, homozygous and heterozygous *Kdm5c* knockout females expressed over double the number  
172 of germline-enriched genes than hemizygous males (Figure 4A). While the majority of germline DEGs in  
173 *Kdm5c*-KO males were also dysregulated in females (74%), many were sex-specific, such as *Tktl2* and *Esx1*  
174 (Figure 4B). We then compared the known functions of germline genes dysregulated only in females, only in  
175 males, or in all samples (Figure 4C). Female-specific germline DEGs were enriched for meiotic (GO:0051321  
176 - meiotic cell cycle) and flagellar (GO:0003341 - cilium movement) functions, while male-specific DEGs had  
177 roles in mitochondrial and cell signaling (GO:0070585 - protein localization to mitochondrion). Germline  
178 transcripts expressed in both sexes were enriched for meiotic (GO:0140013 - meiotic nuclear division) and  
179 egg-specific functions (GO:0007292 - female gamete generation).

180 The majority of germline genes expressed in both sexes were more highly dysregulated in females  
181 compared to males (Figure 4D-F). This increased degree of dysregulation in females, along with the  
182 increased total number of germline genes, indicates females are more sensitive to losing KDM5C-mediated  
183 germline gene suppression. Female sensitivity could be due to impaired XCI in *Kdm5c* mutants<sup>41</sup>, as many  
184 spermatogenesis genes lie on the X chromosome<sup>52,53</sup>. However, female germline DEGs were not biased  
185 towards the X chromosome and had a similar overall proportion of X chromosome DEGs compared to  
186 males (XY *Kdm5c*-KO - 10.29%, XX *Kdm5c*-HET - 7.43%, XX *Kdm5c*-KO - 10.59%) (Figure 4G). The  
187 majority of germline DEGs instead lie on autosomes for both male and female *Kdm5c* mutants (Figure 4G).  
188 Thus, while female EpiLCs are more prone to germline gene misexpression with KDM5C loss, it is likely  
189 independent of XCI defects.

190 **Germline gene misexpression in *Kdm5c* mutants is independent of germ cell sex**

191 Although many germline genes have shared functions in the male and female germline, e.g. PGC  
192 formation, meiosis, and genome defense, some have unique or sex-biased expression. Therefore, we  
193 wondered if *Kdm5c* mutant males would primarily express sperm genes while mutant females would primarily  
194 express egg genes. To comprehensively assess whether germline gene sex corresponds with *Kdm5c* mutant  
195 sex, we first filtered our list of germline-enriched genes for egg and sperm-biased genes (Figure 4H). We

196 defined germ cell sex-biased genes as those whose expression in the opposite sex, at any time point, is no  
197 greater than 20% of the gene's maximum expression in a given sex. This criteria yielded 67 egg-biased,  
198 1,024 sperm-biased, and 197 unbiased germline-enriched genes. We found regardless of sex, egg, sperm,  
199 and unbiased germline genes were dysregulated in all *Kdm5c* mutants at similar proportions (Figure 4I-J).  
200 Furthermore, germline genes dysregulated exclusively in either male or female mutants were also not biased  
201 towards their corresponding germ cell sex (Figure 4I). Altogether, these results demonstrate sex differences  
202 in germline gene dysregulation is not due to sex-specific activation of sperm or egg transcriptional programs.

### 203 **KDM5C binds to a subset of germline gene promoters during early embryogenesis**

204 KDM5C binds to the promoters of several germline genes in embryonic stem cells (ESCs) but not in  
205 neurons<sup>13,54</sup>. However, the lack of a comprehensive list of germline-enriched genes prohibited genome-wide  
206 characterization of KDM5C binding at germline gene promoters. Thus, it is unclear if KDM5C is enriched at  
207 germline gene promoters, what types of germline genes KDM5C regulates, and if its binding is maintained at  
208 any germline genes in neurons.

209 To address these questions, we analyzed KDM5C chromatin immunoprecipitation followed by DNA  
210 sequencing (ChIP-seq) datasets in EpiLCs<sup>41</sup> and primary forebrain neuron cultures (PNCs)<sup>12</sup>. EpiLCs had a  
211 higher total number of high-confidence KDM5C peaks than PNCs (EpiLCs: 5,808, PNCs: 1,276, MACS2 q <  
212 0.1 and fold enrichment > 1). KDM5C was primarily localized to gene promoters in both cell types (Promoters  
213 = transcription start site (TSS) ± 500bp, EpiLCs: 4,190, PNCs: 745), although PNCs showed increased  
214 localization to non-promoter regions (Figure 5A).

215 The majority of promoters bound by KDM5C in PNCs were also bound in EpiLCs (513 shared promoters),  
216 however a large portion of gene promoters were bound by KDM5C only in EpiLCs (3,677 EpiLC only  
217 promoters) (Figure 5B). Genes bound by KDM5C in both PNCs and EpiLCs were enriched for functions  
218 involving nucleic acid turnover, such as deoxyribonucleotide metabolic process (GO:0009262, p.adjust =  
219 8.28e-05) (Figure 5C). Germline-specific ontologies were enriched only in EpiLC-specific KDM5C-bound  
220 promoters, such as meiotic nuclear division (GO: 0007127 p.adjust = 6.77e-16) (Figure 5C). There were no  
221 ontologies significantly enriched for PNC-specific KDM5C target genes. Using our mouse germline gene  
222 list, we observed evident KDM5C signal around the TSS of many germline genes in EpiLCs, but not in  
223 PNCs (Figure 5D). Based on our ChIP-seq peak cut-off criteria, KDM5C was highly enriched at 211 germline  
224 gene promoters in EpiLCs (16.4% of all germline genes) (Figure 5E). Of note, KDM5C was only bound to  
225 about one third of RNA-seq DEG promoters unique to EpiLCs or the brain (EpiLC only DEGs: 34.9%, Brain  
226 only DEGs: 30%) (Supplementary figure 1A-C). Representative examples of KDM5C-bound and unbound  
227 EpiLC DEGs are *Dazl* and *Stra8*, respectively (Figure 5F). However, the four of the five germline genes  
228 dysregulated in both EpiLCs and the brain were bound by KDM5C in EpiLCs (*D1Pas1*, *Hsf2bp*, *Cyct*, and  
229 *Stk31*) (Supplementary figure 1A). Together, these results demonstrate KDM5C is recruited to a subset of  
230 germline genes in EpiLCs, including meiotic genes, but does not directly regulate germline genes in neurons.

231 Furthermore, the majority of germline mRNAs expressed in *Kdm5c*-KO cells are dysregulated independent of  
232 direct KDM5C recruitment to their gene promoters, but genes dysregulated across *Kdm5c*-KO development  
233 are often direct KDM5C targets.

234 Many germline-specific genes are suppressed by the polycomb repressive complex 1.6 (PRC1.6), which  
235 contains transcription factor heterodimers E2F6/DP1 and MGA/MAX that respectively bind E2F and E-box  
236 motifs<sup>57</sup>. PRC1.6 members may recruit KDM5C to germline gene promoters<sup>13</sup>, given their association  
237 with KDM5C in HeLa cells and ESCs<sup>45,58</sup>. We thus used HOMER<sup>59</sup> to identify transcription factor motifs  
238 enriched at KDM5C-bound or unbound germline gene promoters (TSS ± 500 bp, q-value < 0.1). MAX  
239 and E2F6 binding sites were significantly enriched at germline genes bound by KDM5C in EpiLCs (MAX  
240 q-value: 0.0068, E2F6 q-value: 0.0673, E2F q-value: 0.0917), but not at germline genes unbound by  
241 KDM5C (Figure 5G). One third of KDM5C-bound promoters contained the consensus sequence for either  
242 E2F6 (E2F, 5'-TCCCGC-3'), MGA (E-box, 5'-CACGTG-3'), or both, but only 17% of KDM5C-unbound genes  
243 contained these motifs (Figure 5H). KDM5C-unbound germline genes were instead enriched for multiple  
244 RFX transcription factor binding sites (RFX q-value < 0.0001, RFX2 q-value < 0.0001, RFX5 q-value <  
245 0.0001) (Figure 5I, Supplementary figure 1D). RFX transcription factors bind X-box motifs<sup>60</sup> to promote  
246 ciliogenesis<sup>61,62</sup> and among them is RFX2, a central regulator of post-meiotic spermatogenesis<sup>63,64</sup>. Although  
247 *Rfx2* is also not a direct target of KDM5C (Supplementary figure 1E), RFX2 mRNA is derepressed in *Kdm5c*-  
248 KO EpiLCs (Figure 5J). Thus, RFX2 is a candidate transcription factor for driving the ectopic expression of  
249 many KDM5C-unbound germline genes in *Kdm5c*-KO cells.

250 **KDM5C is recruited to CpG islands at germline promoters to facilitate *de novo* DNA  
251 methylation**

252 Previous work found two germline gene promoters have a marked reduction in DNA CpG methylation  
253 (CpGme) in the *Kdm5c*-KO adult hippocampus<sup>13</sup>. Since histone 3 lysine 4 di- and trimethylation (H3K4me2/3)  
254 impede *de novo* CpGme<sup>65,66</sup>, KDM5C's removal of H3K4me2/3 may be required to suppress germline  
255 genes. However, KDM5C's catalytic activity was recently shown to be dispensable for suppressing *Dazl* in  
256 undifferentiated ESCs<sup>45</sup>. To reconcile these observations, we hypothesized KDM5C erases H3K4me2/3 to  
257 promote the initial placement of CpGme at germline gene promoters in EpiLCs.

258 To test this hypothesis, we first characterized KDM5C's expression as naïve ESCs differentiate into  
259 EpiLCs (Figure 6A). While *Kdm5c* mRNA steadily decreased from 0 to 48 hours of differentiation (Figure  
260 6B), KDM5C protein initially increased from 0 to 24 hours but then decreased to near knockout levels by 48  
261 hours (Figure 6C). We then characterized KDM5C's substrates (H3K4me2/3) at germline gene promoters  
262 with *Kdm5c* loss using published ChIP-seq datasets<sup>21,41</sup>. *Kdm5c*-KO samples showed a marked increase in  
263 H3K4me2 in EpiLCs (Figure 6D) and H3K4me3 in the amygdala (Figure 6E) around the TSS of germline  
264 genes. Together, these data suggest KDM5C acts during the transition between ESCs and EpiLCs to remove

265 H3K4me2/3 at germline gene promoters.  
266 Germline genes accumulate CpG methylation (CpGme) at CpG islands (CGIs) during the transition  
267 from naïve to primed pluripotency<sup>18,20,67</sup>. We first examined how many of our germline-enriched genes had  
268 promoter CGIs (TSS ± 500 bp) using the UCSC genome browser<sup>68</sup>. Notably, out of 1,288 germline-enriched  
269 genes, only 356 (27.64%) had promoter CGIs (Figure 6F). CGI-containing germline genes had higher  
270 enrichment of meiotic gene ontologies compared to CGI-free genes, including meiotic nuclear division  
271 (GO:0140013, p.adjust = 2.17e-12) and meiosis I (GO:0007127, p.adjust = 3.91e-10) (Figure 6G). Germline  
272 genes with promoter CGIs were more highly expressed than CGI-free genes across spermatogenesis  
273 stages, with highest expression in meiotic spermatocytes (Figure 6H). Contrastingly, CGI-free genes only  
274 displayed substantial expression in post-meiotic round spermatids (Figure 6H). Although only a minor portion  
275 of germline gene promoters contained CGIs, CGIs strongly determined KDM5C's recruitment to germline  
276 genes ( $p = 2.37e-67$ , Odds Ratio = 17.8, Fisher's exact test), with 79.15% of KDM5C-bound germline gene  
277 promoters harboring CGIs (Figure 6F).

278 To assess how KDM5C loss impacts initial CpGme placement at germline gene promoters, we performed  
279 whole genome bisulfite sequencing (WGBS) in male wild-type and *Kdm5c*-KO ESCs and 96-hour extend  
280 EpiLCs (exEpiLCs), when germline genes reach peak methylation levels<sup>17</sup> (Figure 6I). We first identified  
281 which germline gene promoters significantly gained CpGme in wild-type cells during nESC to exEpiLCs  
282 differentiation (methylKit<sup>69</sup>,  $q < 0.01$ ,  $|methylation\ difference| > 25\%$ , TSS ± 500 bp). In wild-type cells, the  
283 majority of germline genes gained substantial CpGme at their promoter during differentiation (60.08%),  
284 regardless if their promoter contained a CGI (Figure 6J).

285 We then identified promoters differentially methylated in wild-type versus *Kdm5c*-KO exEpiLCs (methylKit,  
286  $q < 0.01$ ,  $|methylation\ difference| > 25\%$ , TSS ± 500 bp). Of the 48,882 promoters assessed, 274 promoters  
287 were significantly hypomethylated and 377 promoters were significantly hypermethylated with KDM5C loss  
288 (Supplementary figure 2A). Many promoters hyper- and hypomethylated in *Kdm5c*-KO exEpiLCs belonged to  
289 genes with unknown functions. Hypomethylated promoters were significantly enriched for germline gene  
290 ontologies, such as meiotic nuclear division (GO:0140013, p.adjust = 0.012) (Supplementary figure 2B),  
291 with 10.22% of hypomethylated promoters belonging to germline genes. Approximately half of germline  
292 promoters hypomethylated in *Kdm5c*-KO exEpiLCs are direct targets of KDM5C in EpiLCs (13 out of 28  
293 hypomethylated promoters).

294 Promoters that showed the most robust loss of CpGme in *Kdm5c*-KO exEpiLCs (lowest q-values) harbored  
295 CGIs (Figure 6K). CGI promoters, but not CGI-free promoters, had a significant reduction in CpGme with  
296 KDM5C loss as a whole (Figure 6L) (Non-CGI promoters  $p = 0.0846$ , CGI promoters  $p = 0.0081$ , Mann-  
297 Whitney U test). Significantly hypomethylated promoters included germline genes consistently dysregulated  
298 across multiple *Kdm5c*-KO RNA-seq datasets<sup>13</sup>, such as *D1Pas1* (methylation difference = -60.03%, q-value  
299 = 3.26e-153) and *Naa11* (methylation difference = -42.45%, q-value = 1.44e-38) (Figure 6M). Surprisingly,  
300 we found only a modest reduction in CpGme at *Dazl*'s promoter (methylation difference = -6.525%, q-value =

301 0.0159) (Figure 6N). Altogether, these results demonstrate KDM5C is recruited to germline gene CGIs in  
302 EpiLCs to promote CpGme at germline gene promoters. Furthermore, this suggests while KDM5C's catalytic  
303 activity is required for the repression of some germline genes, CpGme can be placed at others even with  
304 elevated H3K4me2/3 around the TSS.

## 305 Discussion

306 In the above study, we demonstrate KDM5C's pivotal role in the development of tissue identity. We first  
307 characterized tissue-enriched genes expressed within the mouse *Kdm5c*-KO brain and identified substantial  
308 derepression of testis, liver, muscle, and ovary-enriched genes. Testis genes significantly enriched within the  
309 *Kdm5c*-KO amygdala and hippocampus are specific to the germline and absent in somatic cells. *Kdm5c*-KO  
310 epiblast-like cells (EpiLCs) aberrantly express key drivers of germline identity and meiosis, including *Dazl* and  
311 *Stra8*, while the adult brain primarily expresses genes important for late spermatogenesis. We demonstrated  
312 that although sex did not influence whether sperm or egg-specific genes were misexpressed, female EpiLCs  
313 are more sensitive to germline gene de-repression with KDM5C loss. Germline genes can become aberrantly  
314 expressed in *Kdm5c*-KO cells via indirect mechanisms, such as activation through ectopic RFX transcription  
315 factors. Finally, we found KDM5C is dynamically regulated during ESC to EpiLC differentiation to promote  
316 long-term germline gene silencing through DNA methylation at CpG islands. Therefore, we propose KDM5C  
317 plays a fundamental role in the development of tissue identity during early embryogenesis, including the  
318 establishment of the soma-germline boundary. By systematically characterizing KDM5C's role in germline  
319 gene repression, we unveiled unique mechanisms governing the misexpression of distinct germline gene  
320 classes within somatic lineages. Ultimately, these data provide molecular footholds which can be exploited to  
321 test the overarching contribution of ectopic germline gene expression upon neurodevelopment.

322 By comparing *Kdm5c* mutant males and females, we revealed germline gene suppression is sexually  
323 dimorphic. While sex did not determine whether egg or sperm-specific genes were dysregulated, it greatly  
324 influenced the degree of germline gene dysregulation. Female EpiLCs are more severely impacted by loss  
325 of KDM5C-mediated germline gene suppression, yet this difference is not due to the increased number of  
326 germline genes on the X chromosome<sup>52,53</sup>. Increased germline gene misexpression in females may be  
327 related to females having a higher dose of KDM5C than males, due to its escape from XCI<sup>48–51</sup>. Intriguingly,  
328 heterozygous knockout females also had over double the number of germline DEGs than hemizygous  
329 knockout males, even though their expression of KDM5C should be roughly equivalent to that of wild-type  
330 males. Males could partially compensate for KDM5C's loss via the Y-chromosome homolog, KDM5D. However,  
331 KDM5D exhibits weaker demethylase activity than KDM5C<sup>8</sup> and has not been reported to regulate germline  
332 gene expression. Altogether, these results suggest germline gene silencing mechanisms differ between  
333 males and females, which warrants further study to elucidate the biological ramifications and underlying  
334 mechanisms.

335 We found KDM5C is largely dispensable for promoting normal gene expression during development, yet  
336 is critical for suppressing ectopic developmental programs. It is important to note that while we highlighted  
337 KDM5C's repression of germline genes, some germline-enriched genes like *Dazl* are also expressed at the  
338 2-cell stage and in naïve ESCs/inner cell mass for their role in pluripotency and self-renewal<sup>40,45,70,71</sup>. These  
339 "self-renewal" germline genes are then silenced during ESC differentiation into epiblast stem cells/EpiLCs<sup>17,18</sup>.  
340 We found that while *Kdm5c*-KO EpiLCs express *Dazl*, they did not express 2-cell-specific genes like *Zscan4c*.  
341 These data suggest the 2-cell-like state reported in *Kdm5c*-KO ESCs<sup>45</sup> likely reflects KDM5C's primary  
342 role in germline gene repression. Germline gene misexpression in *Kdm5c*-KO EpiLCs may indicate they  
343 are differentiating into primordial germ cell-like cells (PGCLCs)<sup>33,34,36</sup>. Yet, *Kdm5c*-KO EpiLCs had normal  
344 cellular morphology and properly expressed markers for primed pluripotency, including *Otx2* which blocks  
345 EpiLC differentiation into PGCs/PGCLCs<sup>72</sup>. In addition to unimpaired EpiLC differentiation, *Kdm5c*-KO gross  
346 brain morphology is overall normal<sup>12</sup> and hardly any brain-specific genes were significantly dysregulated in  
347 the amygdala and hippocampus. Thus, ectopic germline gene expression occurs in conjunction with overall  
348 proper somatic differentiation in *Kdm5c*-KO animals.

349 Our work provides novel insight into the cross-talk between H3K4me2/3 and CpGme, which are generally  
350 mutually exclusive<sup>73</sup>. In EpiLCs, loss of KDM5C binding at a subset of germline gene promoters, e.g. *D1Pas1*,  
351 strongly impaired CGI methylation and resulted in their long-lasting de-repression into adulthood. Removal of  
352 H3K4me2/3 at CGIs is a plausible mechanism for KDM5C-mediated germline gene suppression<sup>13,54</sup>, given  
353 H3K4me2/3 can oppose DNMT3 activity<sup>65,66</sup>. However, emerging work indicates many histone-modifying  
354 enzymes have non-catalytic functions that influence gene expression, sometimes even more potently than their  
355 catalytic roles<sup>74,75</sup>. Indeed, KDM5C's catalytic activity was recently found to be dispensable for repressing  
356 *Dazl* in ESCs<sup>45</sup>. In our study, *Dazl*'s promoter still gained CpGme in *Kdm5c*-KO exEpiLCs, even with  
357 elevated H3K4me2. *Dazl* and a few other germline genes employ multiple repressive mechanisms to  
358 facilitate CpGme, such as DNMT3A/B recruitment via E2F6 and MGA<sup>16,17,46,47</sup>. This suggests alternative  
359 silencing mechanisms are sufficient to recruit DNMT3s to some germline CGIs, while others may require  
360 KDM5C-mediated H3K4me removal to overcome promoter CGI escape from CpGme<sup>73,76</sup>. Furthermore,  
361 these results indicate the requirement for KDM5C's catalytic activity can change depending upon the locus  
362 and developmental stage, even for the same class of genes. However, further experiments are required to  
363 determine if catalytically inactive KDM5C can suppress germline genes at later developmental stages.

364 By generating a comprehensive list of mouse germline-enriched genes, we were able to reveal distinct  
365 derepressive mechanisms governing early versus late-stage germline developmental programs. Previous  
366 work on germline gene silencing has focused on genes with promoter CGIs<sup>18,73</sup>, and indeed the major-  
367 ity of KDM5C targets in EpiLCs were germ cell identity genes harboring CGIs. However, over 70% of  
368 germline-enriched gene promoters lacked CGIs, including the many KDM5C-unbound germline genes  
369 that are de-repressed in *Kdm5c*-KO cells. CGI-free, KDM5C-unbound germline genes were primarily  
370 late-stage spermatogenesis genes and significantly enriched for RFX2 binding sites, a central regulator

371 of spermiogenesis<sup>63,64</sup>. These data suggest that once activated during early embryogenesis, drivers of  
372 germline identity like *Rfx2*, *Stra8*, and *Dazl* turn on downstream germline programs, ultimately culminating in  
373 the expression of spermiogenesis genes in the adult *Kdm5c*-KO brain. Therefore, we propose KDM5C is  
374 recruited via promoter CGIs to act as a break against runaway activation of germline-specific programs.

375 The above work provides the mechanistic foundation for KDM5C-mediated repression of tissue and  
376 germline-specific genes. However, the contribution of these ectopic, tissue-specific genes towards *Kdm5c*-  
377 KO neurological impairments is still unknown. In addition to germline genes, we also identified significant  
378 enrichment of muscle and liver-biased transcripts within the *Kdm5c*-KO brain. Intriguingly, select liver and  
379 muscle-biased DEGs do have known roles within the brain, such as the liver-enriched lipid metabolism gene  
380 *Apolipoprotein C-I (Apoc1)*<sup>27</sup>. *APOC1* dysregulation is implicated in Alzheimer's disease in humans<sup>28</sup> and  
381 overexpression of *Apoc1* in the mouse brain can impair learning and memory<sup>77</sup>. KDM5C may therefore be  
382 crucial for neurodevelopment by fine-tuning the expression of tissue-enriched, dosage-sensitive genes like  
383 *Apoc1*.

384 Given germline genes have no known functions within the brain, their impact upon neurodevelopment  
385 is currently unknown. In *C. elegans*, somatic misexpression of germline genes via loss of *Retinoblastoma*  
386 (*Rb*) homologs results in enhanced piRNA signaling and ectopic P granule formation in neurons<sup>78,79</sup>. Ectopic  
387 testicular germline transcripts have also been observed in a variety of cancers, including brain tumors in  
388 *Drosophila* and mammals<sup>80,81</sup> and shown to promote cancer progression<sup>82-84</sup>. Intriguingly, mouse models  
389 and human cells for other chromatin-linked NDDs also display impaired soma-germline demarcation<sup>85-87</sup>,  
390 such as mutations in DNA methyltransferase 3b (DNMT3B), H3K9me1/2 methyltransferases G9A/GLP, and  
391 methyl-CpG -binding protein 2 (MECP2)<sup>85</sup>. Recently, the transcription factor ZMYM2 (ZNF198), whose  
392 mutation causes neurodevelopmental-craniofacial syndrome with variable renal and cardiac abnormalities  
393 (OMIM #619522), was also shown to repress germline genes by promoting H3K4 methylation removal and  
394 CpGme<sup>88</sup>. Thus, KDM5C is among a growing cohort of neurodevelopmental disorders with erosion of the  
395 germline-soma boundary. Further research is required to determine the impact of these germline genes  
396 upon neuronal functions and the extent to which this phenomenon occurs in humans.

## 397 Materials and Methods

### 398 Classifying tissue-enriched and germline-enriched genes

399 Tissue-enriched differentially expressd genes (DEGs) were determined by their classification in a previ-  
400 ously published dataset from 17 male and female mouse tissues<sup>22</sup>. This study defined tissue expression as  
401 greater than 1 Fragments Per Kilobase of transcript per Million mapped read (FPKM) and tissue enrichment  
402 as at least 4-fold higher expression than any other tissue.

403 We curated a list of germline-enriched genes using an RNA-seq dataset from wild-type and germline-

404 depleted (*Kit<sup>W/Wv</sup>*) male and female mouse embryos from embryonic day 12, 14, and 16<sup>32</sup>, as well as adult  
405 male testes<sup>29</sup>. Germline-enriched genes met the following criteria: 1) their expression is greater than 1  
406 FPKM in wild-type germline 2) their expression in any wild-type somatic tissues<sup>22</sup> does not exceed 20%  
407 of maximum expression in wild-type germline, and 3) their expression in the germ cell-depleted (*Kit<sup>W/Wv</sup>*)  
408 germline, for any sex or time point, does not exceed 20% of maximum expression in wild-type germline. We  
409 defined sperm and egg-biased genes as those whose expression in the opposite sex, at any time point, is no  
410 greater than 20% of the gene's maximum expression in a given sex. Genes that did not meet this threshold  
411 for either sex were classified as 'unbiased'.

## 412 Cell culture

413 We utilized our previously established cultures of male wild-type and *Kdm5c* knockout (-KO) embryonic  
414 stem cells<sup>41</sup>. Sex was confirmed by genotyping *Uba1/Uba1y* on the X and Y chromosomes with the following  
415 primers: 5'-TGGATGGTGTGCCAATG-3', 5'-CACCTGCACGTTGCCCTT-3'. Deletion of *Kdm5c* was  
416 confirmed through the primers 5'-ATGCCCATATTAAAGAGTCCTG-3', 5'-TCTGCCTTGATGGGACTGTT-3',  
417 and 5'-GGTTCTAACACTCACATAGTG-3'.

418 Embryonic stem cells (ESCs) and epiblast-like cells were cultured using previously established  
419 methods<sup>37</sup>. Briefly, ESCs were initially cultured in primed ESC (pESC) media consisting of KnockOut  
420 DMEM (Gibco#10829–018), fetal bovine serum (Gibco#A5209501), KnockOut serum replacement  
421 (Invitrogen#10828–028), Glutamax (Gibco#35050-061), Anti-Anti (Gibco#15240-062), MEM Non-essential  
422 amino acids (Gibco#11140-050), and beta-mercaptoethanol (Sigma#M7522). They were then transitioned  
423 into ground-state, "naïve" ESCs (nESCs) by culturing for four passages in N2B27 media containing  
424 DMEM/F12 (Gibco#11330–032), Neurobasal media (Gibco#21103–049), Gluamax (Gibco#35050-061),  
425 Anti-Anti (Gibco#15240-062), N2 supplement (Invitrogen#17502048), and B27 supplement without vitamin  
426 A (Invitrogen#12587-010), and beta-mercaptoethanol. Both pESC and nESC media were supplemented  
427 with 3  $\mu$ M GSK3 inhibitor CHIR99021 (Sigma #SML1046-5MG), 1  $\mu$ M MEK inhibitor PD0325901 (Sigma  
428 #PZ0162-5MG), and 1,000 units/mL leukemia inhibitory factor (LIF, Millipore#ESG1107).

429 nESCs were differentiated into epiblast-like cells (EpiLCs, 48 hours) and extendend EpiLCs (exEpiLCs,  
430 96 hours) by culturing in N2B27 media containing DMEM/F12, Neurobasal media, Gluamax, Anti-Anti,  
431 N2 supplement, B27 supplement (Invitrogen#17504044), beta-mercaptoethanol, fibroblast growth factor 2  
432 (FGF2, R&D Biotechne 233-FB), and activin A (R&D Biotechne 338AC050CF), as previously described<sup>37</sup>.

## 433 Real time quantitative PCR (RT-qPCR)

434 nESCs were differentiated into EpiLCs as described above. Cells were lysed with Tri-reagent BD (Sigma  
435 #T3809) at 0, 24, and 48 hours of differentiation. RNA was phase separated with 0.1 uL/uL 1-bromo-3-  
436 chloropropane (Sigma #B9673) and then precipitated with with isopropanol (Sigma #I9516). For each sample,

437 2 ug of RNA was reverse transcribed using the ProtoScript II Reverse transcriptase kit from New England  
438 Biolabs (NEB #M0368S) and primed with oligo dT. Expression of *Kdm5c* was detected using the primers  
439 5'-CCCATGGAGGCCAGAGAATAAG-3' 5'-CTCAGCGATAAGAGAATTGCTAC-3' and normalized to TBP  
440 using the primers 5'-TTCAGAGGATGCTCTAGGAAGA-3' 5'-CTGTGGAGTAAGTCCTGTGCC-3' with the  
441 Power SYBR™ Green PCR Master Mix (ThermoFisher #4367659).

#### 442 **Western Blot**

443 Total protein was extracted during nESC to EpiLC differentiation at 0, 24, and 48 hours by sonicating cells  
444 at 20% amplitude for 15 seconds in 2X SDS sample buffer, then boiling at 100 °C for 10 minutes. Proteins  
445 were separated on a 7.5% SDS page gel, transferred overnight onto a fluorescent membrane, blotted for  
446 rabbit anti-KDM5C (in house, 1:500) and mouse anti-DAXX (Santa Cruz #(H-7): sc-8043, 1:500) imaged  
447 using the LiCor Odyssey CLx system. Band intensity was quantified using ImageJ.

#### 448 **RNA sequencing (RNA-seq) data analysis**

449 After ensuring read quality via FastQC (v0.11.8), reads were then mapped to the mm10 *Mus musculus*  
450 genome (Gencode) using STAR (v2.5.3a), during which we removed duplicates and kept only uniquely  
451 mapped reads. Count files were generated by FeatureCounts (Subread v1.5.0), and BAM files were  
452 converted to bigwigs using deeptools (v3.1.3) and visualized by the UCSC genome browser. RStudio (v3.6.0)  
453 was then used to analyze counts files by DESeq2 (v1.26.0)<sup>23</sup> to identify differentially expressed genes  
454 (DEGs) with a q-value (p-adjusted via FDR/Benjamini–Hochberg correction) less than 0.1 and a log2 fold  
455 change greater than 0.5. For all DESeq2 analyses, log2 fold changes were calculated with IfcShrink using  
456 the ashR package<sup>89</sup>. MA-plots were generated by ggpibr (v0.6.0), and Eulerr diagrams were generated by  
457 eulerr (v6.1.1). Boxplots and scatterplots were generated by ggpibr (v0.6.0) and ggplot2 (v3.3.2). The Upset  
458 plot was generated via the package UpSetR (v1.4.0)<sup>90</sup>. Gene ontology (GO) analyses were performed by  
459 the R package enrichPlot (v1.16.2) using the biological processes setting and compareCluster.

#### 460 **Chromatin immunoprecipitation followed by DNA sequencing (ChIP-seq) data analysis**

461 ChIP-seq reads were aligned to mm10 using Bowtie1 (v1.1.2) allowing up to two mismatches. Only  
462 uniquely mapped reads were used for analysis. Peaks were called using MACS2 software (v2.2.9.1) using  
463 input BAM files for normalization, with filters for a q-value < 0.1 and a fold enrichment > 1. We removed  
464 “black-listed” genomic regions that often give aberrant signals. Common peak sets were obtained in R via  
465 DiffBind[estrogen@ross-innesDifferentialOestrogenReceptor2012] (v3.6.5). In the case of KDM5C ChIP-seq,  
466 *Kdm5c*-KO peaks were then subtracted from wild-type samples using bedtools (v2.25.0). Peak proximity  
467 to genome annotations was determined by ChIPSeeker<sup>91</sup> (v1.32.1). Gene ontology (GO) analyses were  
468 performed by the R package enrichPlot (v1.16.2) using the biological processes setting and compareCluster.

469 Enriched motifs were identified using HOMER<sup>59</sup>. Average binding across the genome was visualized using  
470 deeptools (v3.1.3). Bigwigs were visualized using the UCSC genome browser.

## 471 **CpG island (CGI) analysis**

472 Locations of CpG islands were determined through the mm10 UCSC genome browser CpG island track<sup>68</sup>,  
473 which classified CGIs as regions that have greater than 50% GC content, are larger than 200 base pairs,  
474 and have a ratio of CG dinucleotides observed over the expected amount greater than 0.6. CGI genomic  
475 coordinates were then annotated using ChIPseeker<sup>91</sup> (v1.32.1) and filtered for ones that lie within promoters  
476 of our germline-enriched genes (TSS ± 500).

## 477 **Whole genome bisulfite sequencing (WGBS)**

478 Genomic DNA (gDNA) from naïve ESCs and extended EpiLCs was extracted using the Wizard Genomic  
479 DNA Purification Kit (Promega A1120), following the instructions for Tissue Culture Cells. gDNA from  
480 two wild-types and two *Kdm5c*-KOs of each cell type was sent to Novogene for WGBS using the Illumina  
481 NovaSeq X Plus platform and sequenced for 150bp paired-end reads (PE150). All samples had greater  
482 than 99% bisulfite conversion rates. Reads were adapter and quality trimmed with Trim Galore (v0.6.10)  
483 and aligned to the mm10 genome using Bismark<sup>92</sup> (v0.22.1). Analysis of differential methylation at germline  
484 gene promoters was performed using methylKit<sup>69</sup> (v1.28.0) with a minimum coverage of 3 paired reads, a  
485 percentage cut-off of 25%, and q-value of 0.01. methylKit was also used to calculate average percentage  
486 methylation at germline gene promoters. Methylation bedgraph tracks were generated via Bismark and  
487 visualized using the UCSC genome browser.

## 488 **Data availability**

### 489 **WGBS in wild-type and *Kdm5c*-KO ESCs and exEpiLCs**

490 XXXX

## 491 **Published datasets**

492 All published datasets are available at the Gene Expression Omnibus (GEO) <https://www.ncbi.nlm.nih.gov/geo>. Published RNA-seq datasets analyzed in this study included the male wild-type and *Kdm5c*-KO  
493 adult amygdala and hippocampus<sup>21</sup> (available at GEO: GSE127722) and male wild-type and *Kdm5c*-KO  
494 EpiLCs<sup>41</sup> (available at GEO: GSE96797).

496 Previously published ChIP-seq experiments included KDM5C in wild-type and *Kdm5c*-KO EpiLCs<sup>41</sup> (avail-  
497 able at GEO: GSE96797) and mouse primary neuron cultures (PNCs) from the cortex and hippocampus<sup>12</sup>  
498 (available at GEO: GSE61036). ChIP-seq of histone 3 lysine 4 dimethylation in male wild-type and *Kdm5c*-KO

499 EpiLCs<sup>41</sup> is also available at GEO: GSE96797. ChIP-seq of histone 3 lysine 4 trimethylation in wild-type and  
500 *Kdm5c*-KO male amygdala<sup>21</sup> are available at GEO: GSE127817.

501 **Data analysis**

502 Scripts used to generate the results, tables, and figures of this study are available via the GitHub  
503 repository: XXX

504 **Acknowledgements**

505 We thank Drs. Sundeep Kalantry, Milan Samanta, and Rebecca Malcore for providing protocols and  
506 expertise in culturing mouse ESCs and EpiLCs, as well as providing the wild-type and *Kdm5c*-KO ESCs  
507 used in this study. We thank Dr. Jacob Mueller for his insight in germline gene regulation and directing us to  
508 the germline-depleted mouse models. We also thank Drs. Gabriel Corfas, Kenneth Kwan, Natalie Tronson,  
509 Michael Sutton, Stephanie Bielas, Donna Martin, and the members of the Iwase, Sutton, Bielas, and Martin  
510 labs for helpful discussions and critiques of the data. We thank members of the University of Michigan  
511 Reproductive Sciences Program for providing feedback throughout the development of this work. This work  
512 was supported by grants from the National Institutes of Health (NIH) (National Institute of Neurological  
513 Disorders and Stroke: NS089896, 5R21NS104774, and NS116008 to S.I.), Farrehi Family Foundation Grant  
514 (to S.I.), the University of Michigan Career Training in Reproductive Biology (NIH T32HD079342, to K.M.B.),  
515 the NIH Early Stage Training in the Neurosciences Training Grant (NIH T32NS076401 to K.M.B.), and the  
516 Michigan Predoctoral Training in Genetics Grant (NIH T32GM007544, to I.V.)

517 **Author contributions**

518 K.M.B. and S.I. conceived the study and designed the experiments. I.V. generated the ESC and exEpiLC  
519 WGBS data. K.M.B performed the data analysis and all other experiments. K.M.B and S.I. wrote and edited  
520 the manuscript.

521 **References**

- 522 1. Strahl, B.D., and Allis, C.D. (2000). The language of covalent histone modifications. *Nature* **403**,  
523 41–45. <https://doi.org/10.1038/47412>.
- 524 2. Jenuwein, T., and Allis, C.D. (2001). Translating the Histone Code. *Science* **293**, 1074–1080.  
525 <https://doi.org/10.1126/science.1063127>.

- 526 3. Lewis, E.B. (1978). A gene complex controlling segmentation in *Drosophila*. *Nature* *276*, 565–570.  
527 <https://doi.org/10.1038/276565a0>.
- 528 4. Kennison, J.A., and Tamkun, J.W. (1988). Dosage-dependent modifiers of polycomb and antennapedia  
529 mutations in *Drosophila*. *Proc. Natl. Acad. Sci. U.S.A.* *85*, 8136–8140. <https://doi.org/10.1073/pnas.85.21.8136>.
- 530 5. Kassis, J.A., Kennison, J.A., and Tamkun, J.W. (2017). Polycomb and Trithorax Group Genes in  
531 *Drosophila*. *Genetics* *206*, 1699–1725. <https://doi.org/10.1534/genetics.115.185116>.
- 532 6. Gabriele, M., Lopez Tobon, A., D'Agostino, G., and Testa, G. (2018). The chromatin basis of  
533 neurodevelopmental disorders: Rethinking dysfunction along the molecular and temporal axes. *Prog  
Neuropsychopharmacol Biol Psychiatry* *84*, 306–327. <https://doi.org/10.1016/j.pnpbp.2017.12.013>.
- 534 7. Schaefer, A., Sampath, S.C., Intrator, A., Min, A., Gertler, T.S., Surmeier, D.J., Tarakhovsky, A.,  
535 and Greengard, P. (2009). Control of cognition and adaptive behavior by the GLP/G9a epigenetic  
suppressor complex. *Neuron* *64*, 678–691. <https://doi.org/10.1016/j.neuron.2009.11.019>.
- 536 8. Iwase, S., Lan, F., Bayliss, P., De La Torre-Ubieta, L., Huarte, M., Qi, H.H., Whetstine, J.R., Bonni, A.,  
537 Roberts, T.M., and Shi, Y. (2007). The X-Linked Mental Retardation Gene SMCX/JARID1C Defines a  
Family of Histone H3 Lysine 4 Demethylases. *Cell* *128*, 1077–1088. <https://doi.org/10.1016/j.cell.2007.02.017>.
- 538 9. Claes, S., Devriendt, K., Van Goethem, G., Roelen, L., Meireleire, J., Raeymaekers, P., Cassiman,  
539 J.J., and Fryns, J.P. (2000). Novel syndromic form of X-linked complicated spastic paraparesis. *Am J  
Med Genet* *94*, 1–4.
- 540 10. Jensen, L.R., Amende, M., Gurok, U., Moser, B., Gimmel, V., Tzschach, A., Janecke, A.R., Tariverdian,  
541 G., Chelly, J., Fryns, J.P., et al. (2005). Mutations in the JARID1C gene, which is involved in  
transcriptional regulation and chromatin remodeling, cause X-linked mental retardation. *Am J Hum  
Genet* *76*, 227–236. <https://doi.org/10.1086/427563>.
- 542 11. Carmignac, V., Nambot, S., Lehalle, D., Callier, P., Moortgat, S., Benoit, V., Ghoumid, J., Delobel,  
543 B., Smol, T., Thuillier, C., et al. (2020). Further delineation of the female phenotype with KDM5C  
disease causing variants: 19 new individuals and review of the literature. *Clin Genet* *98*, 43–55.  
<https://doi.org/10.1111/cge.13755>.
- 544 12. Iwase, S., Brookes, E., Agarwal, S., Badeaux, A.I., Ito, H., Vallianatos, C.N., Tomassy, G.S., Kasza, T.,  
545 Lin, G., Thompson, A., et al. (2016). A Mouse Model of X-linked Intellectual Disability Associated with  
Impaired Removal of Histone Methylation. *Cell Reports* *14*, 1000–1009. <https://doi.org/10.1016/j.celrep.2015.12.091>.

- 546 13. Scandaglia, M., Lopez-Atalaya, J.P., Medrano-Fernandez, A., Lopez-Cascales, M.T., Del Blanco, B.,  
Lipinski, M., Benito, E., Olivares, R., Iwase, S., Shi, Y., et al. (2017). Loss of Kdm5c Causes Spurious  
Transcription and Prevents the Fine-Tuning of Activity-Regulated Enhancers in Neurons. *Cell Rep* **21**,  
47–59. <https://doi.org/10.1016/j.celrep.2017.09.014>.
- 547
- 548 14. Devlin, D.K., Ganley, A.R.D., and Takeuchi, N. (2023). A pan-metazoan view of germline-soma  
distinction challenges our understanding of how the metazoan germline evolves. *Current Opinion in  
Systems Biology* **36**, 100486. <https://doi.org/10.1016/j.coisb.2023.100486>.
- 549
- 550 15. Lehmann, R. (2012). Germline Stem Cells: Origin and Destiny. *Cell Stem Cell* **10**, 729–739.  
<https://doi.org/10.1016/j.stem.2012.05.016>.
- 551
- 552 16. Endoh, M., Endo, T.A., Shinga, J., Hayashi, K., Farcas, A., Ma, K.W., Ito, S., Sharif, J., Endoh, T.,  
Onaga, N., et al. (2017). PCGF6-PRC1 suppresses premature differentiation of mouse embryonic  
stem cells by regulating germ cell-related genes. *eLife* **6**. <https://doi.org/10.7554/eLife.21064>.
- 553
- 554 17. Mochizuki, K., Sharif, J., Shirane, K., Uranishi, K., Bogutz, A.B., Janssen, S.M., Suzuki, A., Okuda,  
A., Koseki, H., and Lorincz, M.C. (2021). Repression of germline genes by PRC1.6 and SETDB1  
in the early embryo precedes DNA methylation-mediated silencing. *Nat Commun* **12**, 7020. <https://doi.org/10.1038/s41467-021-27345-x>.
- 555
- 556 18. Borgel, J., Guibert, S., Li, Y., Chiba, H., Schübeler, D., Sasaki, H., Forné, T., and Weber, M. (2010).  
Targets and dynamics of promoter DNA methylation during early mouse development. *Nat Genet* **42**,  
1093–1100. <https://doi.org/10.1038/ng.708>.
- 557
- 558 19. Velasco, G., Hubé, F., Rollin, J., Neuillet, D., Philippe, C., Bouzinba-Segard, H., Galvani, A., Viegas-  
Péquignot, E., and Francastel, C. (2010). Dnmt3b recruitment through E2F6 transcriptional repressor  
mediates germ-line gene silencing in murine somatic tissues. *Proc Natl Acad Sci U S A* **107**, 9281–  
9286. <https://doi.org/10.1073/pnas.1000473107>.
- 559
- 560 20. Hackett, J.A., Reddington, J.P., Nestor, C.E., Dunican, D.S., Branco, M.R., Reichmann, J., Reik,  
W., Surani, M.A., Adams, I.R., and Meehan, R.R. (2012). Promoter DNA methylation couples  
genome-defence mechanisms to epigenetic reprogramming in the mouse germline. *Development*  
**139**, 3623–3632. <https://doi.org/10.1242/dev.081661>.
- 561
- 562 21. Vallianatos, C.N., Raines, B., Porter, R.S., Bonefas, K.M., Wu, M.C., Garay, P.M., Collette, K.M.,  
Seo, Y.A., Dou, Y., Keegan, C.E., et al. (2020). Mutually suppressive roles of KMT2A and KDM5C  
in behaviour, neuronal structure, and histone H3K4 methylation. *Commun Biol* **3**, 278. <https://doi.org/10.1038/s42003-020-1001-6>.
- 563
- 564 22. Li, B., Qing, T., Zhu, J., Wen, Z., Yu, Y., Fukumura, R., Zheng, Y., Gondo, Y., and Shi, L. (2017). A  
Comprehensive Mouse Transcriptomic BodyMap across 17 Tissues by RNA-seq. *Sci Rep* **7**, 4200.  
<https://doi.org/10.1038/s41598-017-04520-z>.
- 565

- 566 23. Love, M.I., Huber, W., and Anders, S. (2014). Moderated estimation of fold change and dispersion for  
567 RNA-seq data with DESeq2. *Genome Biol* 15, 550. <https://doi.org/10.1186/s13059-014-0550-8>.
- 568 24. Crackower, M.A., Kolas, N.K., Noguchi, J., Sarao, R., Kikuchi, K., Kaneko, H., Kobayashi, E., Kawai, Y.,  
569 Kozieradzki, I., Landers, R., et al. (2003). Essential Role of Fkbp6 in Male Fertility and Homologous  
Chromosome Pairing in Meiosis. *Science* 300, 1291–1295. <https://doi.org/10.1126/science.1083022>.
- 570 25. Xiol, J., Cora, E., Koglgruber, R., Chuma, S., Subramanian, S., Hosokawa, M., Reuter, M., Yang, Z.,  
Berninger, P., Palencia, A., et al. (2012). A Role for Fkbp6 and the Chaperone Machinery in piRNA  
Amplification and Transposon Silencing. *Molecular Cell* 47, 970–979. <https://doi.org/10.1016/j.molcel.2012.07.019>.
- 572 26. Cheng, S., Altmeppen, G., So, C., Welp, L.M., Penir, S., Ruhwedel, T., Menelaou, K., Harasimov, K.,  
Stützer, A., Blayney, M., et al. (2022). Mammalian oocytes store mRNAs in a mitochondria-associated  
573 membraneless compartment. *Science* 378, eabq4835. <https://doi.org/10.1126/science.abq4835>.
- 574 27. Rouland, A., Masson, D., Lagrost, L., Vergès, B., Gautier, T., and Bouillet, B. (2022). Role of  
apolipoprotein C1 in lipoprotein metabolism, atherosclerosis and diabetes: A systematic review.  
575 *Cardiovasc Diabetol* 21, 272. <https://doi.org/10.1186/s12933-022-01703-5>.
- 576 28. Leduc, V., Jasmin-Bélanger, S., and Poirier, J. (2010). APOE and cholesterol homeostasis in  
Alzheimer's disease. *Trends in Molecular Medicine* 16, 469–477. <https://doi.org/10.1016/j.molmed.2010.07.008>.
- 578 29. Mueller, J.L., Skaletsky, H., Brown, L.G., Zaghloul, S., Rock, S., Graves, T., Auger, K., Warren,  
W.C., Wilson, R.K., and Page, D.C. (2013). Independent specialization of the human and mouse X  
579 chromosomes for the male germ line. *Nat Genet* 45, 1083–1087. <https://doi.org/10.1038/ng.2705>.
- 580 30. Handel, M.A., and Eppig, J.J. (1979). Sertoli Cell Differentiation in the Testes of Mice Genetically  
Deficient in Germ Cells. *Biology of Reproduction* 20, 1031–1038. <https://doi.org/10.1095/biolreprod20.5.1031>.
- 582 31. Green, C.D., Ma, Q., Manske, G.L., Shami, A.N., Zheng, X., Marini, S., Moritz, L., Sultan, C.,  
Gurczynski, S.J., Moore, B.B., et al. (2018). A Comprehensive Roadmap of Murine Spermatogenesis  
Defined by Single-Cell RNA-Seq. *Dev Cell* 46, 651–667.e10. <https://doi.org/10.1016/j.devcel.2018.07.025>.
- 584 32. Soh, Y.Q., Junker, J.P., Gill, M.E., Mueller, J.L., van Oudenaarden, A., and Page, D.C. (2015). A  
Gene Regulatory Program for Meiotic Prophase in the Fetal Ovary. *PLoS Genet* 11, e1005531.  
585 <https://doi.org/10.1371/journal.pgen.1005531>.
- 586 33. Magnúsdóttir, E., and Surani, M.A. (2014). How to make a primordial germ cell. *Development* 141,  
587 245–252. <https://doi.org/10.1242/dev.098269>.

- 588 34. Günesdogan, U., Magnúsdóttir, E., and Surani, M.A. (2014). Primordial germ cell specification: A  
context-dependent cellular differentiation event [corrected]. *Philos Trans R Soc Lond B Biol Sci* **369**.  
<https://doi.org/10.1098/rstb.2013.0543>.
- 589 35. Bardot, E.S., and Hadjantonakis, A.-K. (2020). Mouse gastrulation: Coordination of tissue patterning,  
specification and diversification of cell fate. *Mechanisms of Development* **163**, 103617. <https://doi.org/10.1016/j.mod.2020.103617>.
- 590 36. Hayashi, K., Ohta, H., Kurimoto, K., Aramaki, S., and Saitou, M. (2011). Reconstitution of the  
mouse germ cell specification pathway in culture by pluripotent stem cells. *Cell* **146**, 519–532.  
<https://doi.org/10.1016/j.cell.2011.06.052>.
- 591 37. Samanta, M., and Kalantry, S. (2020). Generating primed pluripotent epiblast stem cells: A methodol-  
ogy chapter. *Curr Top Dev Biol* **138**, 139–174. <https://doi.org/10.1016/bs.ctdb.2020.01.005>.
- 592 38. Welling, M., Chen, H., Muñoz, J., Musheev, M.U., Kester, L., Junker, J.P., Mischerikow, N., Arbab, M.,  
Kuijk, E., Silberstein, L., et al. (2015). DAZL regulates Tet1 translation in murine embryonic stem cells.  
*EMBO Reports* **16**, 791–802. <https://doi.org/10.15252/embr.201540538>.
- 593 39. Macfarlan, T.S., Gifford, W.D., Driscoll, S., Lettieri, K., Rowe, H.M., Bonanomi, D., Firth, A., Singer, O.,  
Trono, D., and Pfaff, S.L. (2012). Embryonic stem cell potency fluctuates with endogenous retrovirus  
activity. *Nature* **487**, 57–63. <https://doi.org/10.1038/nature11244>.
- 594 40. Suzuki, A., Hirasaki, M., Hishida, T., Wu, J., Okamura, D., Ueda, A., Nishimoto, M., Nakachi, Y.,  
Mizuno, Y., Okazaki, Y., et al. (2016). Loss of MAX results in meiotic entry in mouse embryonic and  
germline stem cells. *Nat Commun* **7**, 11056. <https://doi.org/10.1038/ncomms11056>.
- 595 41. Samanta, M.K., Gayen, S., Harris, C., Maclary, E., Murata-Nakamura, Y., Malcore, R.M., Porter, R.S.,  
Garay, P.M., Vallianatos, C.N., Samollow, P.B., et al. (2022). Activation of Xist by an evolutionarily  
conserved function of KDM5C demethylase. *Nat Commun* **13**, 2602. <https://doi.org/10.1038/s41467-022-30352-1>.
- 596 42. Koubova, J., Menke, D.B., Zhou, Q., Capel, B., Griswold, M.D., and Page, D.C. (2006). Retinoic  
acid regulates sex-specific timing of meiotic initiation in mice. *Proc. Natl. Acad. Sci. U.S.A.* **103**,  
2474–2479. <https://doi.org/10.1073/pnas.0510813103>.
- 597 43. Lin, Y., Gill, M.E., Koubova, J., and Page, D.C. (2008). Germ Cell-Intrinsic and -Extrinsic Factors  
Govern Meiotic Initiation in Mouse Embryos. *Science* **322**, 1685–1687. <https://doi.org/10.1126/science.1166340>.
- 598 44. Endo, T., Mikedis, M.M., Nicholls, P.K., Page, D.C., and De Rooij, D.G. (2019). Retinoic Acid and Germ  
Cell Development in the Ovary and Testis. *Biomolecules* **9**, 775. <https://doi.org/10.3390/biom9120775>.

- 610 45. Gupta, N., Yakhou, L., Albert, J.R., Azogui, A., Ferry, L., Kirsh, O., Miura, F., Battault, S., Yamaguchi, K., Laisné, M., et al. (2023). A genome-wide screen reveals new regulators of the 2-cell-like cell state. Nat Struct Mol Biol. <https://doi.org/10.1038/s41594-023-01038-z>.
- 611
- 612 46. Pohlers, M., Truss, M., Frede, U., Scholz, A., Strehle, M., Kuban, R.-J., Hoffmann, B., Morkel, M., Birchmeier, C., and Hagemann, C. (2005). A Role for E2F6 in the Restriction of Male-Germ-Cell-Specific Gene Expression. Current Biology 15, 1051–1057. <https://doi.org/10.1016/j.cub.2005.04.060>.
- 613
- 614 47. Dahlet, T., Truss, M., Frede, U., Al Adhami, H., Bardet, A.F., Dumas, M., Vallet, J., Chicher, J., Hammann, P., Kottnik, S., et al. (2021). E2F6 initiates stable epigenetic silencing of germline genes during embryonic development. Nat Commun 12, 3582. <https://doi.org/10.1038/s41467-021-23596-w>.
- 615
- 616 48. Agulnik, A.I., Mitchell, M.J., Mattei, M.G., Borsani, G., Avner, P.A., Lerner, J.L., and Bishop, C.E. (1994). A novel X gene with a widely transcribed Y-linked homologue escapes X-inactivation in mouse and human. Hum Mol Genet 3, 879–884. <https://doi.org/10.1093/hmg/3.6.879>.
- 617
- 618 49. Carrel, L., Hunt, P.A., and Willard, H.F. (1996). Tissue and lineage-specific variation in inactive X chromosome expression of the murine Smcx gene. Hum Mol Genet 5, 1361–1366. <https://doi.org/10.1093/hmg/5.9.1361>.
- 619
- 620 50. Sheardown, S., Norris, D., Fisher, A., and Brockdorff, N. (1996). The mouse Smcx gene exhibits developmental and tissue specific variation in degree of escape from X inactivation. Hum Mol Genet 5, 1355–1360. <https://doi.org/10.1093/hmg/5.9.1355>.
- 621
- 622 51. Xu, J., Deng, X., and Disteche, C.M. (2008). Sex-Specific Expression of the X-Linked Histone Demethylase Gene Jarid1c in Brain. PLoS ONE 3, e2553. <https://doi.org/10.1371/journal.pone.0002553>.
- 623
- 624 52. Wang, P.J., McCarrey, J.R., Yang, F., and Page, D.C. (2001). An abundance of X-linked genes expressed in spermatogonia. Nat Genet 27, 422–426. <https://doi.org/10.1038/86927>.
- 625
- 626 53. Khil, P.P., Smirnova, N.A., Romanienko, P.J., and Camerini-Otero, R.D. (2004). The mouse X chromosome is enriched for sex-biased genes not subject to selection by meiotic sex chromosome inactivation. Nat Genet 36, 642–646. <https://doi.org/10.1038/ng1368>.
- 627
- 628 54. Al Adhami, H., Vallet, J., Schaal, C., Schumacher, P., Bardet, A.F., Dumas, M., Chicher, J., Hammann, P., Daujat, S., and Weber, M. (2023). Systematic identification of factors involved in the silencing of germline genes in mouse embryonic stem cells. Nucleic Acids Research 51, 3130–3149. <https://doi.org/10.1093/nar/gkad071>.
- 629
- 630 55. Hurlin, P.J. (1999). Mga, a dual-specificity transcription factor that interacts with Max and contains a T-domain DNA-binding motif. The EMBO Journal 18, 7019–7028. <https://doi.org/10.1093/emboj/18.2.7019>.
- 631

- 632 56. Tatsumi, D., Hayashi, Y., Endo, M., Kobayashi, H., Yoshioka, T., Kiso, K., Kanno, S., Nakai, Y., Maeda, I., Mochizuki, K., et al. (2018). DNMTs and SETDB1 function as co-repressors in MAX-mediated repression of germ cell-related genes in mouse embryonic stem cells. *PLoS ONE* *13*, e0205969. <https://doi.org/10.1371/journal.pone.0205969>.
- 633
- 634 57. Stielow, B., Finkernagel, F., Stiewe, T., Nist, A., and Suske, G. (2018). MGA, L3MBTL2 and E2F6 determine genomic binding of the non-canonical Polycomb repressive complex PRC1.6. *PLoS Genet* *14*, e1007193. <https://doi.org/10.1371/journal.pgen.1007193>.
- 635
- 636 58. Tahiliani, M., Mei, P., Fang, R., Leonor, T., Rutenberg, M., Shimizu, F., Li, J., Rao, A., and Shi, Y. (2007). The histone H3K4 demethylase SMCX links REST target genes to X-linked mental retardation. *Nature* *447*, 601–605. <https://doi.org/10.1038/nature05823>.
- 637
- 638 59. Heinz, S., Benner, C., Spann, N., Bertolino, E., Lin, Y.C., Laslo, P., Cheng, J.X., Murre, C., Singh, H., and Glass, C.K. (2010). Simple Combinations of Lineage-Determining Transcription Factors Prime cis-Regulatory Elements Required for Macrophage and B Cell Identities. *Molecular Cell* *38*, 576–589. <https://doi.org/10.1016/j.molcel.2010.05.004>.
- 639
- 640 60. Gajiwala, K.S., Chen, H., Cornille, F., Roques, B.P., Reith, W., Mach, B., and Burley, S.K. (2000). Structure of the winged-helix protein hRFX1 reveals a new mode of DNA binding. *Nature* *403*, 916–921. <https://doi.org/10.1038/35002634>.
- 641
- 642 61. Swoboda, P., Adler, H.T., and Thomas, J.H. (2000). The RFX-Type Transcription Factor DAF-19 Regulates Sensory Neuron Cilium Formation in *C. elegans*. *Molecular Cell* *5*, 411–421. [https://doi.org/10.1016/S1097-2765\(00\)80436-0](https://doi.org/10.1016/S1097-2765(00)80436-0).
- 643
- 644 62. Ashique, A.M., Choe, Y., Karlen, M., May, S.R., Phamluong, K., Solloway, M.J., Ericson, J., and Peterson, A.S. (2009). The Rfx4 Transcription Factor Modulates Shh Signaling by Regional Control of Ciliogenesis. *Sci. Signal.* *2*. <https://doi.org/10.1126/scisignal.2000602>.
- 645
- 646 63. Kistler, W.S., Baas, D., Lemeille, S., Paschaki, M., Seguin-Estevez, Q., Barras, E., Ma, W., Duteyrat, J.-L., Morlé, L., Durand, B., et al. (2015). RFX2 Is a Major Transcriptional Regulator of Spermiogenesis. *PLoS Genet* *11*, e1005368. <https://doi.org/10.1371/journal.pgen.1005368>.
- 647
- 648 64. Wu, Y., Hu, X., Li, Z., Wang, M., Li, S., Wang, X., Lin, X., Liao, S., Zhang, Z., Feng, X., et al. (2016). Transcription Factor RFX2 Is a Key Regulator of Mouse Spermiogenesis. *Sci Rep* *6*, 20435. <https://doi.org/10.1038/srep20435>.
- 649
- 650 65. Otani, J., Nankumo, T., Arita, K., Inamoto, S., Ariyoshi, M., and Shirakawa, M. (2009). Structural basis for recognition of H3K4 methylation status by the DNA methyltransferase 3A ATRX–DNMT3–DNMT3L domain. *EMBO Reports* *10*, 1235–1241. <https://doi.org/10.1038/embor.2009.218>.
- 651

- 652 66. Guo, X., Wang, L., Li, J., Ding, Z., Xiao, J., Yin, X., He, S., Shi, P., Dong, L., Li, G., et al. (2015).  
653 Structural insight into autoinhibition and histone H3-induced activation of DNMT3A. *Nature* **517**,  
640–644. <https://doi.org/10.1038/nature13899>.
- 654 67. Meissner, A., Mikkelsen, T.S., Gu, H., Wernig, M., Hanna, J., Sivachenko, A., Zhang, X., Bernstein,  
655 B.E., Nusbaum, C., Jaffe, D.B., et al. (2008). Genome-scale DNA methylation maps of pluripotent and  
differentiated cells. *Nature* **454**, 766–770. <https://doi.org/10.1038/nature07107>.
- 656 68. Nassar, L.R., Barber, G.P., Benet-Pagès, A., Casper, J., Clawson, H., Diekhans, M., Fischer, C.,  
657 Gonzalez, J.N., Hinrichs, A.S., Lee, B.T., et al. (2023). The UCSC Genome Browser database: 2023  
update. *Nucleic Acids Research* **51**, D1188–D1195. <https://doi.org/10.1093/nar/gkac1072>.
- 658 69. Akalin, A., Kormaksson, M., Li, S., Garrett-Bakelman, F.E., Figueiroa, M.E., Melnick, A., and Mason,  
659 C.E. (2012). methylKit: A comprehensive R package for the analysis of genome-wide DNA methylation  
profiles. *Genome Biol* **13**, R87. <https://doi.org/10.1186/gb-2012-13-10-r87>.
- 660 70. Torres-Padilla, M.-E. (2020). On transposons and totipotency. *Philos Trans R Soc Lond B Biol Sci*  
661 **375**, 20190339. <https://doi.org/10.1098/rstb.2019.0339>.
- 662 71. Yang, M., Yu, H., Yu, X., Liang, S., Hu, Y., Luo, Y., Izsvák, Z., Sun, C., and Wang, J. (2022). Chemical-  
induced chromatin remodeling reprograms mouse ESCs to totipotent-like stem cells. *Cell Stem Cell*  
663 **29**, 400–418.e13. <https://doi.org/10.1016/j.stem.2022.01.010>.
- 664 72. Zhang, J., Zhang, M., Acampora, D., Vojtek, M., Yuan, D., Simeone, A., and Chambers, I. (2018).  
OTX2 restricts entry to the mouse germline. *Nature* **562**, 595–599. <https://doi.org/10.1038/s41586-018-0581-5>.
- 666 73. Weber, M., Hellmann, I., Stadler, M.B., Ramos, L., Pääbo, S., Rebhan, M., and Schübeler, D. (2007).  
667 Distribution, silencing potential and evolutionary impact of promoter DNA methylation in the human  
genome. *Nat Genet* **39**, 457–466. <https://doi.org/10.1038/ng1990>.
- 668 74. Aubert, Y., Egolf, S., and Capell, B.C. (2019). The Unexpected Noncatalytic Roles of Histone Modifiers  
in Development and Disease. *Trends in Genetics* **35**, 645–657. <https://doi.org/10.1016/j.tig.2019.06.004>.
- 670 75. Morgan, M.A.J., and Shilatifard, A. (2020). Reevaluating the roles of histone-modifying enzymes  
and their associated chromatin modifications in transcriptional regulation. *Nat Genet* **52**, 1271–1281.  
671 <https://doi.org/10.1038/s41588-020-00736-4>.
- 672 76. Long, H.K., King, H.W., Patient, R.K., Odom, D.T., and Klose, R.J. (2016). Protection of CpG  
islands from DNA methylation is DNA-encoded and evolutionarily conserved. *Nucleic Acids Res* **44**,  
673 6693–6706. <https://doi.org/10.1093/nar/gkw258>.

- 674 77. Abildayeva, K., Berbée, J.F.P., Blokland, A., Jansen, P.J., Hoek, F.J., Meijer, O., Lütjohann, D., Gautier, T., Pillot, T., De Vente, J., et al. (2008). Human apolipoprotein C-I expression in mice impairs learning and memory functions. *Journal of Lipid Research* *49*, 856–869. <https://doi.org/10.1194/jlr.M700518JLR200>.
- 675
- 676 78. Wang, D., Kennedy, S., Conte, D., Kim, J.K., Gabel, H.W., Kamath, R.S., Mello, C.C., and Ruvkun, G. (2005). Somatic misexpression of germline P granules and enhanced RNA interference in retinoblastoma pathway mutants. *Nature* *436*, 593–597. <https://doi.org/10.1038/nature04010>.
- 677
- 678 79. Wu, X., Shi, Z., Cui, M., Han, M., and Ruvkun, G. (2012). Repression of germline RNAi pathways in somatic cells by retinoblastoma pathway chromatin complexes. *PLoS Genet* *8*, e1002542. <https://doi.org/10.1371/journal.pgen.1002542>.
- 679
- 680 80. Nielsen, A.Y., and Gjerstorff, M.F. (2016). Ectopic Expression of Testis Germ Cell Proteins in Cancer and Its Potential Role in Genomic Instability. *Int J Mol Sci* *17*. <https://doi.org/10.3390/ijms17060890>.
- 681
- 682 81. Adebayo Babatunde, K., Najafi, A., Salehipour, P., Modarressi, M.H., and Mobasher, M.B. (2017). Cancer/Testis genes in relation to sperm biology and function. *Iranian Journal of Basic Medical Sciences* *20*. <https://doi.org/10.22038/ijbms.2017.9259>.
- 683
- 684 82. Janic, A., Mendizabal, L., Llamazares, S., Rossell, D., and Gonzalez, C. (2010). Ectopic expression of germline genes drives malignant brain tumor growth in *Drosophila*. *Science* *330*, 1824–1827. <https://doi.org/10.1126/science.1195481>.
- 685
- 686 83. Ghafouri-Fard, S., and Modarressi, M.-H. (2012). Expression of Cancer–Testis Genes in Brain Tumors: Implications for Cancer Immunotherapy. *Immunotherapy* *4*, 59–75. <https://doi.org/10.2217/imt.11.145>.
- 687
- 688 84. Nin, D.S., and Deng, L.-W. (2023). Biology of Cancer-Testis Antigens and Their Therapeutic Implications in Cancer. *Cells* *12*, 926. <https://doi.org/10.3390/cells12060926>.
- 689
- 690 85. Bonefas, K.M., and Iwase, S. (2021). Soma-to-germline transformation in chromatin-linked neurodevelopmental disorders? *FEBS J*. <https://doi.org/10.1111/febs.16196>.
- 691
- 692 86. Velasco, G., Walton, E.L., Sterlin, D., Hédouin, S., Nitta, H., Ito, Y., Fouyssac, F., Mégarbané, A., Sasaki, H., Picard, C., et al. (2014). Germline genes hypomethylation and expression define a molecular signature in peripheral blood of ICF patients: Implications for diagnosis and etiology. *Orphanet J Rare Dis* *9*, 56. <https://doi.org/10.1186/1750-1172-9-56>.
- 693
- 694 87. Walton, E.L., Francastel, C., and Velasco, G. (2014). Dnmt3b Prefers Germ Line Genes and Centromeric Regions: Lessons from the ICF Syndrome and Cancer and Implications for Diseases. *Biology (Basel)* *3*, 578–605. <https://doi.org/10.3390/biology3030578>.
- 695

- 696 88. Graham-Paquin, A.-L., Saini, D., Sirois, J., Hossain, I., Katz, M.S., Zhuang, Q.K.-W., Kwon, S.Y.,  
Yamanaka, Y., Bourque, G., Bouchard, M., et al. (2023). ZMYM2 is essential for methylation of  
germline genes and active transposons in embryonic development. *Nucleic Acids Research*, gkad540.  
697 <https://doi.org/10.1093/nar/gkad540>.
- 698 89. Stephens, M. (2016). False discovery rates: A new deal. *Biostat*, kxw041. <https://doi.org/10.1093/biostatistics/kxw041>.
- 700 90. Conway, J.R., Lex, A., and Gehlenborg, N. (2017). UpSetR: An R package for the visualization of  
intersecting sets and their properties. *Bioinformatics* 33, 2938–2940. <https://doi.org/10.1093/bioinformatics/btx364>.
- 701 91. Yu, G., Wang, L.G., and He, Q.Y. (2015). ChIPseeker: An R/Bioconductor package for ChIP peak  
annotation, comparison and visualization. *Bioinformatics* 31, 2382–2383. <https://doi.org/10.1093/bioinformatics/btv145>.
- 702 92. Krueger, F., and Andrews, S.R. (2011). Bismark: A flexible aligner and methylation caller for Bisulfite-  
Seq applications. *Bioinformatics* 27, 1571–1572. <https://doi.org/10.1093/bioinformatics/btr167>.
- 703
- 704
- 705

706 **Figures and Tables**

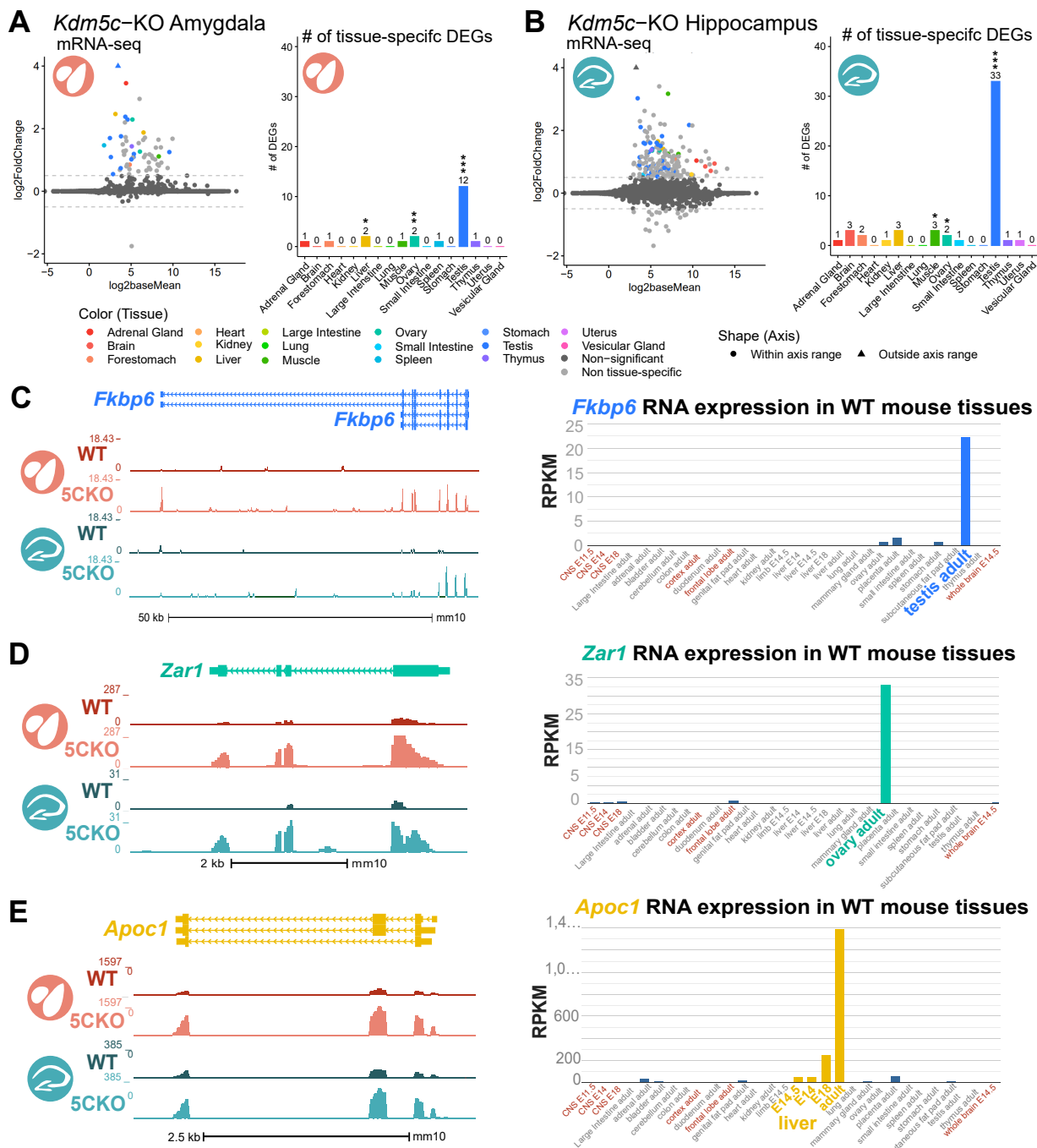


**Figure 1: Tissue-enriched genes are misexpressed in the *Kdm5c*-KO brain.** **A-B.** Expression of tissue-enriched genes (Li et al 2017) in the male *Kdm5c*-KO amygdala (A) and hippocampus (B). Left - MA plot of mRNA-sequencing. Right - Number of tissue-enriched differentially expressed genes (DEGs). \*  $p < 0.05$ , \*\*  $p < 0.01$ , \*\*\*  $p < 0.001$ , Fisher's exact test. **C.** Left - UCSC browser view of an example aberrantly expressed testis-enriched DEG, *FK506 binding protein 6* (*Fkbp6*) in the wild-type (WT) and *Kdm5c*-KO (5CKO) amygdala (red) and hippocampus (teal) (Average,  $n = 4$ ). Right - Expression of *Cyct* in wild-type tissues from NCBI Gene, with testis highlighted in blue and brain tissues highlighted in red. **D.** Left - UCSC browser view of an example ovary-enriched DEG, *Zygotic arrest 1* (*Zar1*). Right - Expression of *Zar1* in wild-type tissues from NCBI Gene, with ovary highlighted in teal and brain tissues highlighted in red. **E.** Left - UCSC browser view of an example liver-enriched DEG, *Apolipoprotein C-I* (*Apoc1*). Right - Expression of *Apoc1* in wild-type tissues from NCBI Gene, with liver highlighted in orange and brain tissues highlighted in red.

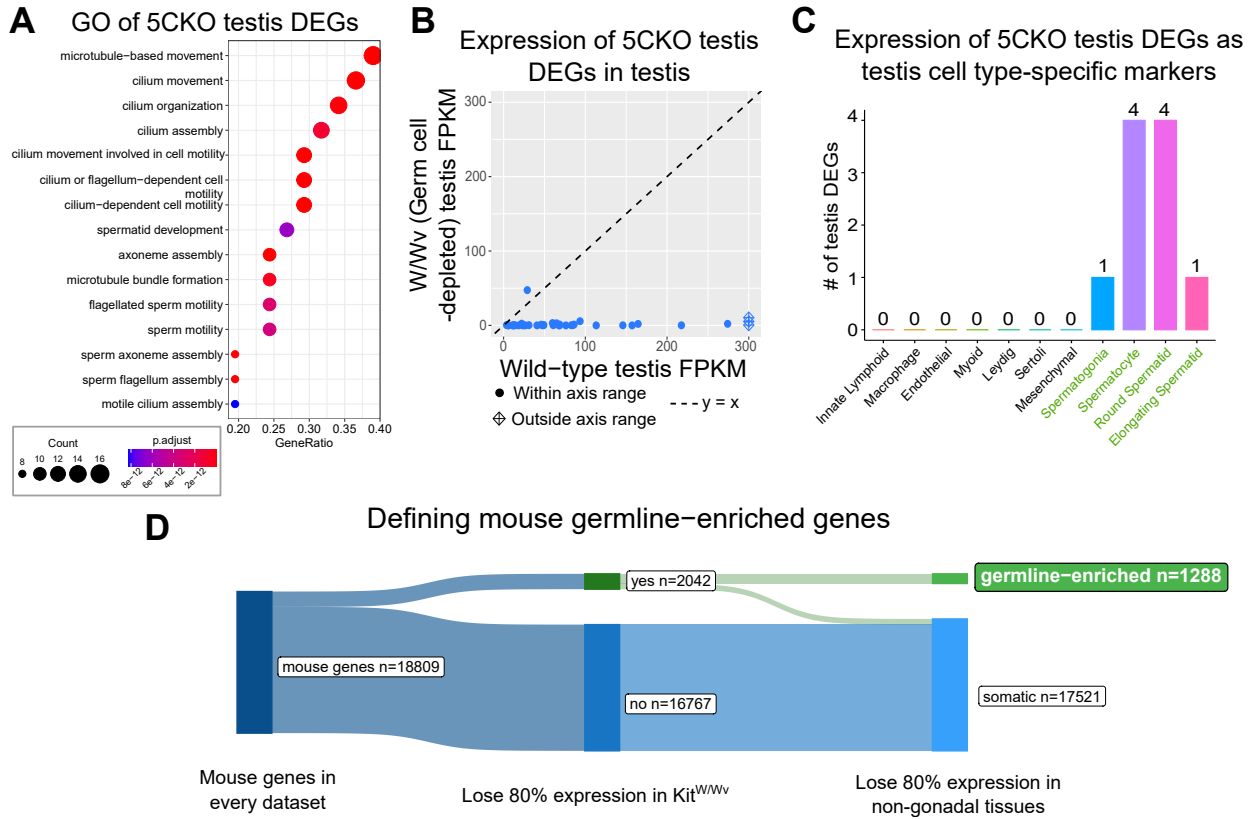


**Figure 2: Aberrant transcription of germline genes in the *Kdm5c*-KO in the brain.** **A.** enrichPlot gene ontology (GO) of *Kdm5c*-KO amygdala and hippocampus testis-enriched DEGs **B.** Expression of testis DEGs in wild-type (WT) versus germ cell-depleted (W/Wv) testis (Mueller et al 2013). Expression is in Fragments Per Kilobase of transcript per Million mapped reads (FPKM). **C.** Number of testis DEGs that were classified as cell-type specific markers in a single cell RNA-seq dataset of the testis (Green et al 2018). Germline cell types are highlighted in green, somatic cell types in black. **D.** Sankey diagram of mouse genes filtered for germline enrichment based on their expression in wild-type and W/Wv mice and in adult mouse non-gonadal tissues (Li et al 2017).

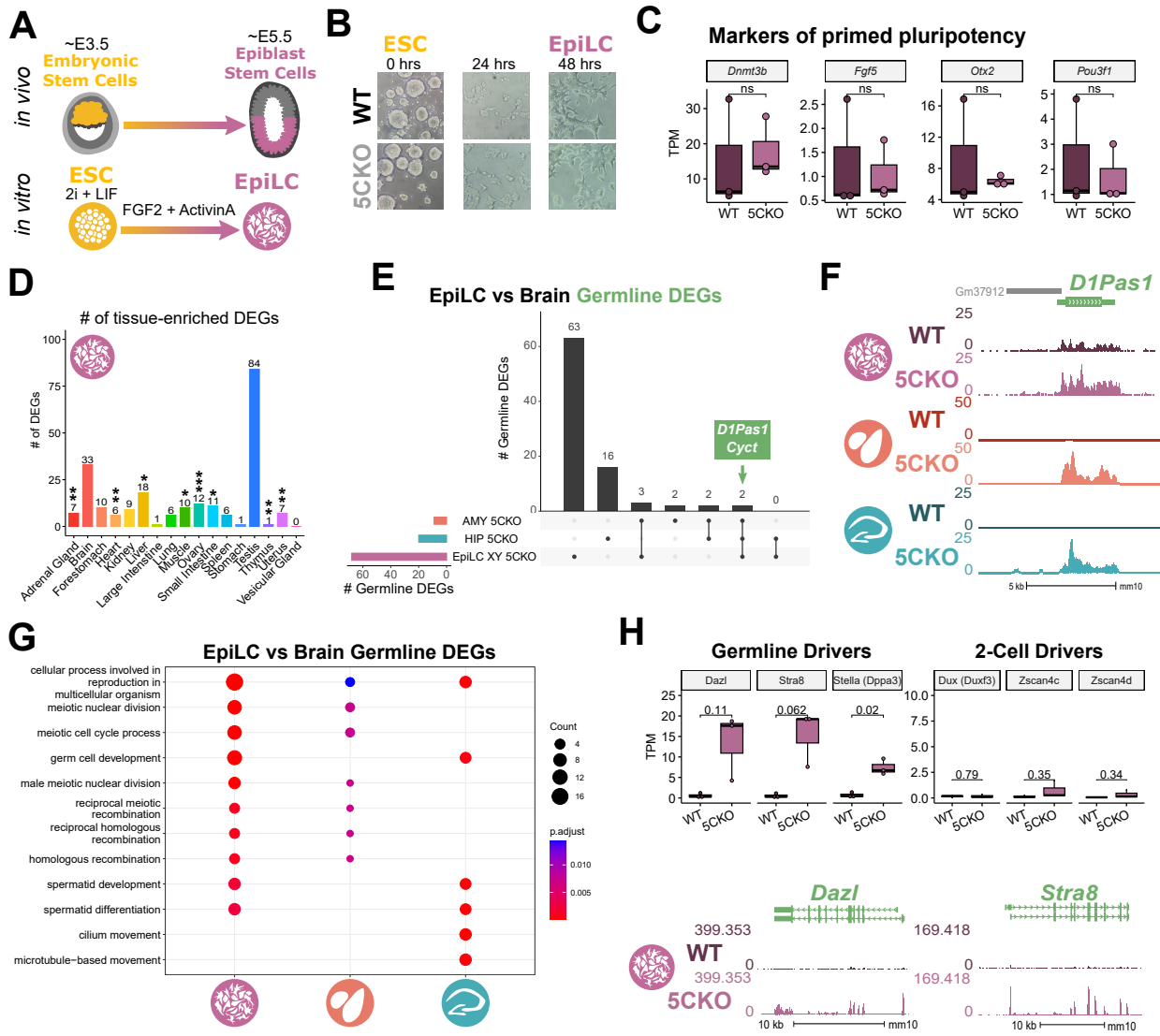


**Figure 3: Kdm5c-KO epiblast-like cells express key drivers of germline identity** **A.** Top - Diagram of *in vivo* differentiation of embryonic stem cells (ESCs) of the inner cell mass into epiblast stem cells. Bottom - *in vitro* differentiation of ESCs into epiblast-like cells (EpiLCs). **B.** Representative images of male wild-type (WT) and *Kdm5c*-KO (5CKO) cells during ESC to EpiLC differentiation. Brightfield images taken at 20X. **C.** No significant difference in primed pluripotency marker expression in wild-type versus *Kdm5c*-KO EpiLCs. Welch's t-test, expression in transcripts per million (TPM). **D.** Number of tissue-enriched differentially expressed genes (DEGs) in *Kdm5c*-KO EpiLCs. \*  $p < 0.05$ , \*\*  $p < 0.01$ , \*\*\*  $p < 0.001$ , Fisher's exact test. **E.** Upset plot displaying the overlap of germline DEGs expressed in *Kdm5c*-KO EpiLCs, amygdala (AMY), and hippocampus (HIP) RNA-seq datasets. **F.** UCSC browser view of an example germline gene, *D1Pas1*, that is dysregulated *Kdm5c*-KO EpiLCs (top, purple. Average,  $n = 3$ ), amygdala (middle, red. Average,  $n = 4$ ), and hippocampus (bottom, blue. Average,  $n = 4$ ). **G.** enrichPlot gene ontology analysis comparing enriched biological processes for *Kdm5c*-KO EpiLC, amygdala, and hippocampus germline DEGs. **H.** Top left - Example germline identity DEGs unique to EpiLCs. Top right - Example 2-cell genes that are not dysregulated in *Kdm5c*-KO EpiLCs. p-values for Welch's t-test. Bottom - UCSC browser view of *Dazl* and *Stra8* expression in wild-type and *Kdm5c*-KO EpiLCs (Average,  $n = 3$ ).

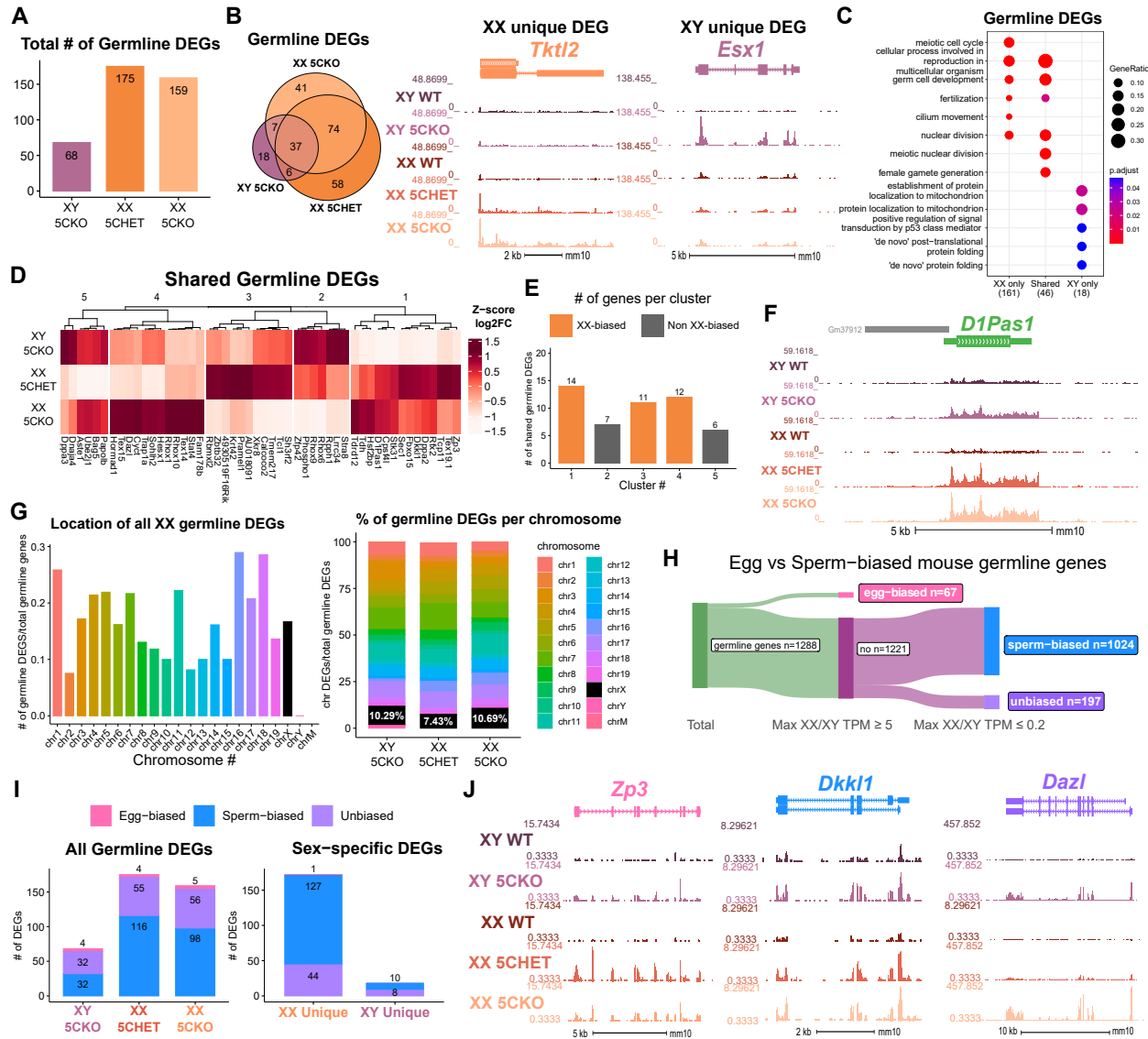


**Figure 4: Chromosomal sex influences *Kdm5c*-KO germline gene misexpression.** **A.** Total number of germline-enriched RNA-seq DEGs for male hemizygous *Kdm5c* knockout EpilCs (XY 5CKO, purple), female heterozygous *Kdm5c* knockout (XX 5CHET, orange), female homozygous *Kdm5c* knockout (XX 5CKO, light orange) EpilCs. **B.** Left - Eulerr overlap of *Kdm5c* mutant male and female EpilC germline DEGs. Right - Example of germline DEGs unique to females or males, *Tktl2* and *Esx1*. **C.** enrichPlot gene ontology analysis comparing enriched biological processes for germline DEGs shared between *Kdm5c* mutant males and females (Shared), or unique to one sex (XX only or XY only). **D.** Heatmap of germline DEGs shared between male and female mutants. Color is the average log 2 fold change from sex-matched wild-type. **E.** Number of genes within each cluster from D. Clusters with higher expression in females compared to males (XX-biased) highlighted in orange. **F.** UCSC browser view of a male and female shared germline DEG *D1Pas1* that is more highly expressed in female mutants (Average, n = 3). **G.** Left - Number of all female germline DEGs located on each chromosome over the total number of germline-enriched genes on that chromosome. Right - Percentage of germline DEGs that lie on each chromosome for each *Kdm5c* mutant. X chromosome highlighted in black. **H.** Sankey diagram classifying egg-biased (pink) and sperm-biased (blue) and unbiased (purple) mouse germline-enriched genes. **I.** Number of egg, sperm, or unbiased germline DEGs for male and female *Kdm5c* mutants. **J.** UCSC browser view of egg-biased (*Zp3*), sperm-biased (*Dkk1*), and unbiased (*Dazl*) germline genes dysregulated in both male and female *Kdm5c* mutants (Average of n = 3).

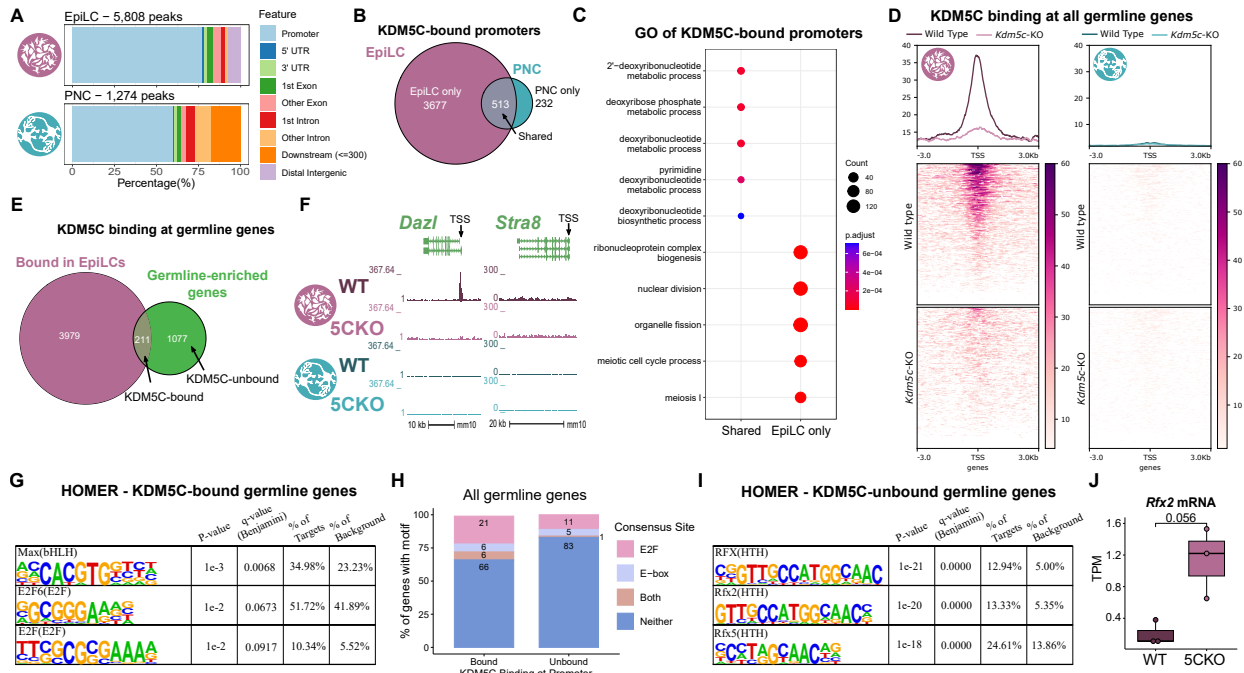


**Figure 5: KDM5C binds to a subset of germline gene promoters during early embryogenesis.** **A.** ChIPseeker localization of KDM5C peaks at different genomic regions in EpiLCs (top) and hippocampal and cortex primary neuron cultures (PNCs, bottom). **B.** Overlap of genes with KDM5C bound to their promoters ( $TSS \pm 500$ ) in EpiLCs (purple) and PNCs (blue). **C.** Gene ontology (GO) comparison of genes with KDM5C bound to their promoter in EpiLCs and PNCs. Genes were classified as either bound in EpiLCs only (EpiLC only), unique to PNCs (PNC only, no significant ontologies) or bound in both PNCs and EpiLCs (Shared). **D.** Average KDM5C binding around the transcription start site (TSS) of all germline-enriched genes in EpiLCs (left) and PNCs (right). **E.** Eulerr overlap of germline-enriched genes (green) with significant KDM5C binding at their promoter in EpiLCs (purple). **F.** Example KDM5C ChIP-seq signal around the *Dazl* TSS but not *Stra8* in EpiLCs. **G.** HOMER motif analysis of all KDM5C-bound germline gene promoters, highlighting significant enrichment of MAX, E2F6, and E2F motifs. **H.** Number of all gene promoters bound or unbound by KDM5C with instances of the E2F or E-box consensus sequence. **I.** HOMER motif analysis of all KDM5C-unbound germline gene promoters, highlighting significant enrichment of RFX family transcription factor motifs. **J.** Expression of RNA-seq DEG *Rfx2* in wild-type and *Kdm5c*-KO EpiLCs. P-value of Welch's t-test, expression in transcripts per million (TPM).

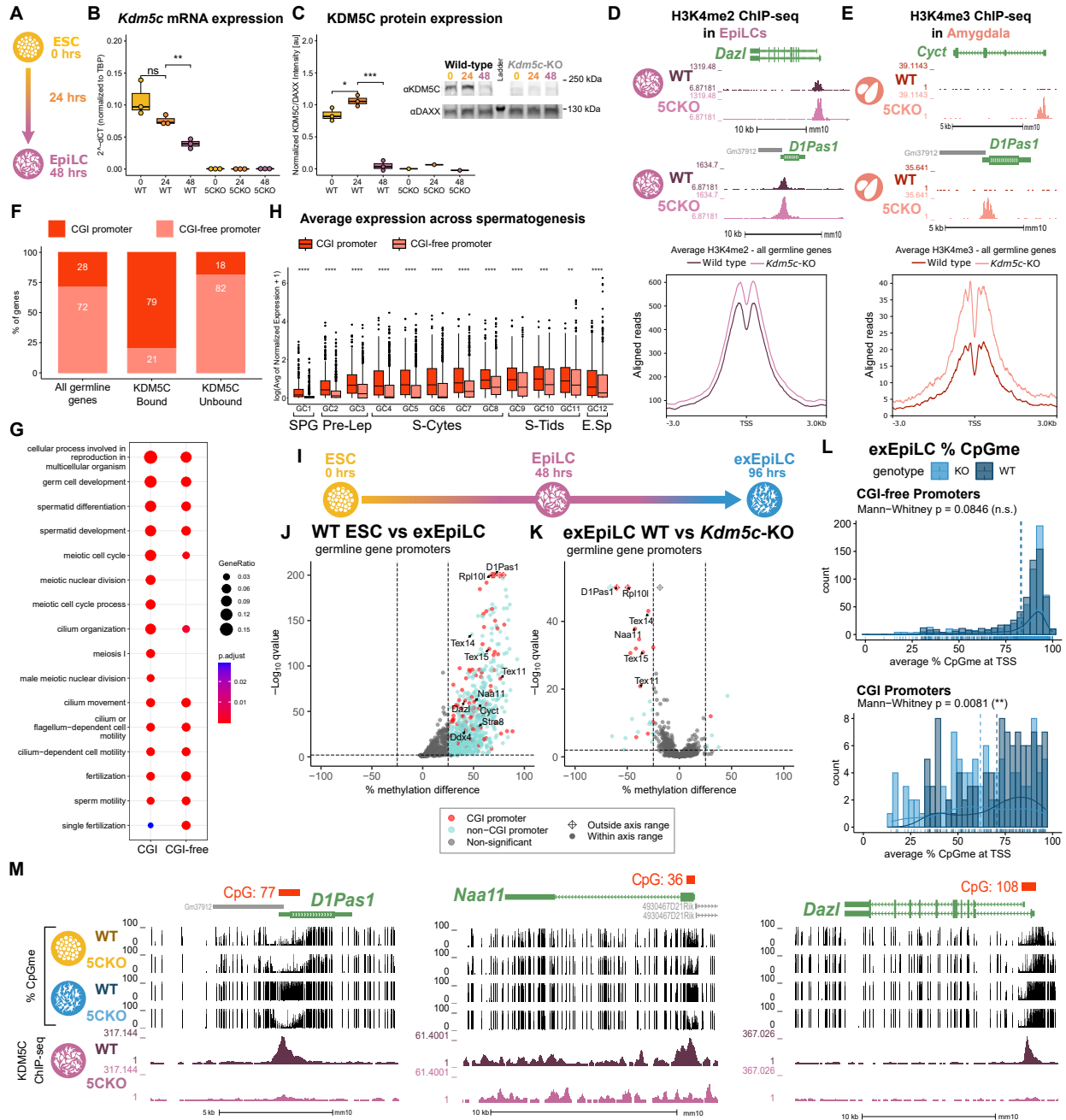


**Figure 6: KDM5C promotes long-term silencing of germline genes via DNA methylation at CpG islands.** **A.** Diagram of embryonic stem cell (ESC) to epiblast-like cell (EpiLC) differentiation and collection time points. **B.** Real time quantitative PCR (RT-qPCR) of *Kdm5c* mRNA expression in wild-type (WT) and *Kdm5c*-KO (5CKO) ESCs at 0, 24, and 48 hours of differentiation into EpiLCs. Expression calculated in comparison to TBP mRNA expression ( $2^{-\Delta\Delta CT}$ ). \*  $p < 0.05$ , \*\*  $p < 0.01$ , \*\*\*  $p < 0.001$ , Welch's t-test. **C.** KDM5C protein expression normalized to DAXX. Quantified intensity using ImageJ (artificial units - au). Right - representative lanes of Western blot for KDM5C and DAXX. \*  $p < 0.05$ , \*\*  $p < 0.01$ , \*\*\*  $p < 0.001$ , Welch's t-test. **D.** Top - Representative UCSC browser view of histone 3 lysine 4 dimethylation (H3K4me2) ChIP-seq signal at two germline genes in wild-type and *Kdm5c*-KO EpiLCs. Bottom - Average H3K4me2 signal at the TSS of all germline-enriched genes in wild-type (dark purple) and *Kdm5c*-KO (light purple) EpiLCs. **E.** Top - Representative UCSC browser view of histone 3 lysine 4 trimethylation (H3K4me3) ChIP-seq signal at two germline genes in the wild-type (WT) and *Kdm5c*-KO (5CKO) adult amygdala. Bottom - Average H3K4me3 signal at the transcription start site (TSS) of all germline-enriched genes in wild-type (dark red) and *Kdm5c*-KO (light red) amygdala. **F.** Percentage of germline genes that harbor CpG islands (CGIs) in their promoters (CGI promoter, red), based on UCSC annotation. Left - percentage of all germline-enriched genes, middle - KDM5C-bound germline genes, and right - KDM5C-unbound germline genes. (Legend continued on next page.)

**Figure 6: KDM5C promotes long-term silencing of germline genes via DNA methylation at CpG islands.** (Legend continued.) **G.** enrichPlot gene ontology analysis of germline genes with (CGI-promoter) or without (CGI-free) CGIs in their promoter. **H.** Expression of germline genes with (CGI-promoter, red) or without (CGI-free, salmon) CGIs in their promoter across stages of spermatogenesis from Green et al 2018. SPG - spermatogonia, Pre-Lep - preleptotene spermatocytes, S-Cytes - meiotic spermatocytes, S-Tids - post-meiotic haploid round spermatids, E.Sp - elongating spermatids. Wilcoxon test, \*  $p < 0.05$ , \*\*  $p < 0.01$ , \*\*\*  $p < 0.001$ , \*\*\*\*  $p < 0.0001$ . **I.** Diagram of ESC to extended EpiLC (exEpiLC) differentiation. **J.** Volcano plot of whole genome bisulfite sequencing (WGBS) comparing CpG methylation (CpGme) at germline gene promoters ( $TSS \pm 500$ ) in wild-type (WT) ESCs versus exEpiLCs. Significantly differentially methylated promoters ( $q < 0.01$ ,  $|methylated difference| > 25\%$ ) with CGIs in red, CGI-free promoters in light blue **K.** Volcano plot of WGBS of wild-type (WT) versus *Kdm5c*-KO exEpiLCs for germline gene promoters. Promoters with CGIs in red, CGI-free promoters in light blue. **L.** Histogram of average percent CpGme at the promoter of germline genes with or without CGIs. Wild-type in navy and *Kdm5c*-KO (KO) in light blue. Dashed lines are average methylation for each genotype, p-values for Mann-Whitney U test. **M.** UCSC browser view of germline genes, showing UCSC annotated CGI with number of CpGs, representative CpGme in wild-type (WT) and *Kdm5c*-KO (5CKO) ESCs and exEpiLCs, and KDM5C ChIP-seq signal in EpiLCs.